Editors' Suggestion

Measurement of $|V_{cb}|$ with $B_s^0 \to D_s^{(*)-}\mu^+\nu_\mu$ decays

R. Aaij *et al.*[*]
(LHCb Collaboration)

(Received 10 January 2020; accepted 9 March 2020; published 20 April 2020)

The element $|V_{cb}|$ of the Cabibbo-Kobayashi-Maskawa matrix is measured using semileptonic B_s^0 decays produced in proton-proton collision data collected with the LHCb detector at center-of-mass energies of 7 and 8 TeV, corresponding to an integrated luminosity of 3 fb^{-1}. Rates of $B_s^0 \to D_s^-\mu^+\nu_\mu$ and $B_s^0 \to D_s^{*-}\mu^+\nu_\mu$ decays are analyzed using hadronic form-factor parametrizations derived either by Caprini, Lellouch and Neubert (CLN) or by Boyd, Grinstein and Lebed (BGL). The measured values of $|V_{cb}|$ are $(41.4 \pm 0.6 \pm 0.9 \pm 1.2) \times 10^{-3}$ and $(42.3 \pm 0.8 \pm 0.9 \pm 1.2) \times 10^{-3}$ in the CLN and BGL parametrization, respectively. The first uncertainty is statistical, the second systematic, and the third is due to the external inputs used in the measurement. These results are in agreement with those obtained from decays of B^+ and B^0 mesons. They are the first determinations of $|V_{cb}|$ at a hadron-collider experiment and the first using B_s^0 meson decays.

DOI: 10.1103/PhysRevD.101.072004

I. INTRODUCTION

The semileptonic quark-level transition $\bar{b} \to \bar{c}\ell^+\nu_\ell$, where ℓ is an electron or a muon, provides the cleanest way to access the strength of the coupling between the b and c quarks, expressed by the element $|V_{cb}|$ of the Cabibbo-Kobayashi-Maskawa (CKM) matrix.[1] Two complementary methods have been used to determine $|V_{cb}|$. One measures the decay rate by looking at *inclusive* b-hadron decays to final states made of a c-flavored hadron and a charged lepton; the other measures the rate of a specific (*exclusive*) decay, such as $B^0 \to D^*(2010)^-\mu^+\nu_\mu$ or $B^0 \to D^-\mu^+\nu_\mu$. The average of the inclusive method yields $|V_{cb}| = (42.19 \pm 0.78) \times 10^{-3}$, while the exclusive determinations give $|V_{cb}| = (39.25 \pm 0.56) \times 10^{-3}$ [1]. The two values are approximately three standard deviations apart, and this represents a long-standing puzzle in flavor physics.

Exclusive determinations rely on a parametrization of strong-interaction effects in the hadronic current of the quarks bound in mesons, the so-called form factors. These are Lorentz-invariant functions of the squared mass q^2 of the virtual W^+ emitted in the $\bar{b} \to \bar{c}$ transition and are calculated using nonperturbative quantum chromodynamics (QCD) techniques, such as lattice QCD (LQCD) or QCD sum rules. Several parametrizations have been proposed to model the form factors [2–7]. The parametrization derived by Caprini, Lellouch and Neubert (CLN) [2] has been the reference model for the exclusive determinations of $|V_{cb}|$. The approximations adopted in this parametrization have been advocated as a possible explanation for the discrepancy with the inclusive measurement [8–11]. A more general model by Boyd, Grinstein and Lebed (BGL) [3–5] has been used in recent high-precision measurements of $|V_{cb}|$ [12,13] to overcome the CLN limitations. However, no significant difference in the $|V_{cb}|$ values measured with the two parametrizations has been found and the issue remains open [14–17].

All exclusive measurements of $|V_{cb}|$ performed so far make use of decays of B^+ and B^0 mesons. The study of other b-hadron decays, which are potentially subject to different sources of uncertainties, can provide complementary information and may shed light on this puzzle. In particular, semileptonic B_s^0 decays, which are abundant at the LHC, have not yet been exploited to measure $|V_{cb}|$. Exclusive semileptonic B_s^0 decays are more advantageous from a theoretical point of view. The larger mass of the valence s quark compared to u or d quarks makes LQCD calculations of the form factors for B_s^0 decays less computationally expensive than those for B^+ or B^0 decays, thus possibly allowing for a more precise determination of $|V_{cb}|$ [18–21]. Calculations of the form factor over the full q^2 spectrum are available for $B_s^0 \to D_s^-\ell^+\nu_\ell$ decays [22,23] and can be used along with experimental data to measure $|V_{cb}|$. Exclusive $B_s^0 \to D_s^-\ell^+\nu_\ell$ and $B_s^0 \to D_s^{*-}\ell^+\nu_\ell$ decays are also experimentally appealing because background

[*]Full author list given at the end of the article.

[1]The inclusion of charge-conjugate processes is implied throughout this paper.

contamination from partially reconstructed decays is expected to be less severe than for their $B^{+/0}$ counterparts. Indeed, the majority of the excited states of the D_s^- meson (other than D_s^{*-}) are expected to decay dominantly into $D^{(*)}K$ final states.

This paper presents the first determination of $|V_{cb}|$ from the exclusive decays $B_s^0 \to D_s^- \mu^+ \nu_\mu$ and $B_s^0 \to D_s^{*-} \mu^+ \nu_\mu$. The analysis uses proton-proton collision data collected with the LHCb detector at center-of-mass energies of 7 and 8 TeV and corresponding to an integrated luminosity of 3 fb^{-1}. In both decays, only the $D_s^- \mu^+$ final state is reconstructed using the Cabibbo-favored mode $D_s^- \to [K^+K^-]_\phi \pi^-$, where the kaon pair is required to have invariant mass in the vicinity of the $\phi(1020)$ resonance. The photon or the neutral pion emitted along with the D_s^- in the D_s^{*-} decay is not reconstructed. The value of $|V_{cb}|$ is determined from the observed yields of B_s^0 decays normalized to those of *reference* B^0 decays after correcting for the relative reconstruction and selection efficiencies. The reference decays are chosen to be $B^0 \to D^- \mu^+ \nu_\mu$ and $B^0 \to D^{*-} \mu^+ \nu_\mu$, where the D^- meson is reconstructed in the Cabibbo-suppressed mode $D^- \to [K^+K^-]_\phi \pi^-$. Hereafter the symbol D^{*-} refers to the $D^*(2010)^-$ meson. Signal and reference decays thus have identical final states and similar kinematic properties. This choice results in a reference sample of smaller size than that of the signal but allows suppressing systematic uncertainties that affect the calculation of the efficiencies. Using the B^0 decays as a reference, the determination of $|V_{cb}|$ needs in input the measured branching fractions of these decays and the ratio of B_s^0- to B^0-meson production fractions. The latter is measured by LHCb using an independent sample of semileptonic decays with respect to that exploited in this analysis [24], and it assumes universality of the semileptonic decay width of b hadrons [25]. The ratios of the branching fractions of signal and reference decays,

$$\mathcal{R} \equiv \frac{\mathcal{B}(B_s^0 \to D_s^- \mu^+ \nu_\mu)}{\mathcal{B}(B^0 \to D^- \mu^+ \nu_\mu)}, \tag{1}$$

$$\mathcal{R}^* \equiv \frac{\mathcal{B}(B_s^0 \to D_s^{*-} \mu^+ \nu_\mu)}{\mathcal{B}(B^0 \to D^{*-} \mu^+ \nu_\mu)}, \tag{2}$$

are also determined from the same analysis. From the measured branching fractions of the reference decays, the branching fractions of $B_s^0 \to D_s^- \mu^+ \nu_\mu$ and $B_s^0 \to D_s^{*-} \mu^+ \nu_\mu$ decays are determined for the first time.

This analysis uses either the CLN or the BGL parametrization to model the form factors, with parameters determined by analyzing the decay rates using a novel method: instead of approximating q^2, which cannot be determined precisely because of the undetected neutrino, a variable that can be reconstructed fully from the final-state particles and that preserves information on the form factors is used. This variable is the component of the D_s^- momentum perpendicular to the B_s^0 flight direction, denoted as $p_\perp(D_s^-)$. The $p_\perp(D_s^-)$ variable is highly correlated with the q^2 value of the $B_s^0 \to D_s^- \mu^+ \nu_\mu$ and $B_s^0 \to D_s^{*-} \mu^+ \nu_\mu$ decays and, to a minor extent, with the helicity angles of the $B_s^0 \to D_s^{*-} \mu^+ \nu_\mu$ decay. When used together with the corrected mass $m_{\rm corr}$, it also helps in determining the sample composition. The corrected mass is calculated from the mass of the reconstructed particles, $m(D_s^- \mu^+)$, and from the momentum of the $D_s^- \mu^+$ system transverse to the B_s^0 flight direction, $p_\perp(D_s^- \mu^+)$, as

$$m_{\rm corr} \equiv \sqrt{m^2(D_s^- \mu^+) + p_\perp^2(D_s^- \mu^+)} + p_\perp(D_s^- \mu^+). \tag{3}$$

Signal and background decays accumulate in well-separated regions of the two-dimensional space spanned by $m_{\rm corr}$ and $p_\perp(D_s^-)$. A fit to the data distribution in the $m_{\rm corr}$ versus $p_\perp(D_s^-)$ plane identifies the $B_s^0 \to D_s^- \mu^+ \nu_\mu$ and $B_s^0 \to D_s^{*-} \mu^+ \nu_\mu$ signal decays and simultaneously provides a measurement of $|V_{cb}|$ and of the form factors.

The paper is structured as follows. The formalism describing the semileptonic $B_{(s)}^0$ decays and the parametrization of their form factors is outlined in Sec. II. Section III gives a brief description of the LHCb detector and of the simulation software. The selection and the expected composition of the signal and reference samples are presented in Sec. IV. Section V describes the method used to measure $|V_{cb}|$ and the other parameters of interest. The determination of the reference B^0-decay yields is reported in Sec. VI, and the analysis of the signal B_s^0 decays is discussed in Sec. VII. Section VIII describes the systematic uncertainties affecting the measurements and Sec. IX presents the final results, before concluding.

II. FORMALISM

The formalism used to describe the decay rate of a B meson into a semileptonic final state with a pseudoscalar or a vector D meson is outlined here. In this section, the notation $B \to D^{(*)} \mu\nu$ is used to identify both $B^0 \to D^{(*)-} \mu^+ \nu_\mu$ and $B_s^0 \to D_s^{(*)-} \mu^+ \nu_\mu$ decays, clarifying when the distinction is relevant.

A. $B \to D^* \mu\nu$ decays

The $B \to D^* \mu\nu$ differential decay rate can be expressed in terms of one recoil variable, w, and three helicity angles, θ_μ, θ_D and χ, as

$$\frac{{\rm d}^4\Gamma(B \to D^* \mu\nu)}{{\rm d}w\, {\rm d}\cos\theta_\mu\, {\rm d}\cos\theta_D\, {\rm d}\chi} = \frac{3 m_B^3 m_{D^*}^2 G_{\rm F}^2}{16(4\pi)^4} \eta_{\rm EW}^2 |V_{cb}|^2 |\mathcal{A}(w, \theta_\mu, \theta_D, \chi)|^2, \tag{4}$$

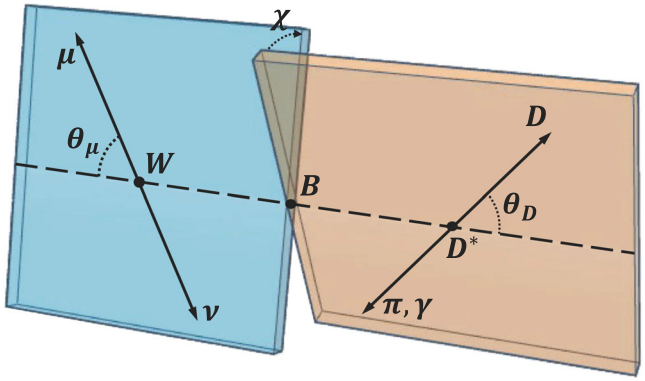

FIG. 1. Graphical representation of the helicity angles in $B \to D^*\mu\nu$ decays. The definitions are provided in the text.

where G_F is the Fermi constant and the coefficient $\eta_{EW} \approx 1.0066$ accounts for the leading-order electroweak correction [26]. The recoil variable is defined as the scalar product of the four-velocities of the B and D^* mesons, $w = v_B \cdot v_{D^*} = (m_B^2 + m_{D^*}^2 - q^2)/(2m_B m_{D^*})$, with $m_{B(D^*)}$ being the mass of the B (D^*) meson. The minimum value $w = 1$ corresponds to zero recoil of the D^* meson in the B rest frame, i.e., the largest kinematically allowed value of q^2. The helicity angles (represented in Fig. 1) are θ_μ, the angle between the direction of the muon in the W rest frame and the direction of the W boson in the B rest frame; θ_D, the angle between the direction of the D in the D^* rest frame and the direction of the D^* in the B rest frame; and χ, the angle between the plane formed by the D^* decay products and that formed by the two leptons. In the limit of massless leptons, the decay amplitude $\mathcal{A}$ can be decomposed in terms of three amplitudes $H_{\pm/0}(w)$, corresponding to the three possible helicity states of the D^* meson, and its squared modulus is written as

$$|\mathcal{A}(w,\theta_\mu,\theta_D,\chi)|^2 = \sum_i^6 \mathcal{H}_i(w) k_i(\theta_\mu,\theta_D,\chi), \quad (5)$$

with the $\mathcal{H}_i$ and k_i terms defined in Table I. The helicity amplitudes are expressed by three form factors, $h_{A_1}(w)$, $R_1(w)$, and $R_2(w)$, as

$$H_{\pm/0}(w) = 2\frac{\sqrt{m_B m_{D^*}}}{m_B + m_{D^*}}(1-r^2)(w+1)(w^2-1)^{1/4} \times h_{A_1}(w)\tilde{H}_{\pm/0}(w), \quad (6)$$

with $r = m_{D^*}/m_B$ and

$$\tilde{H}_\pm(w) = \frac{\sqrt{1-2wr+r^2}}{1-r}\left[1 \mp \sqrt{\frac{w-1}{w+1}}R_1(w)\right], \quad (7)$$

$$\tilde{H}_0(w) = 1 + \frac{(w-1)(1-R_2(w))}{1-r}. \quad (8)$$

The CLN parametrization uses dispersion relations and reinforced unitarity bounds based on heavy quark effective theory to derive simplified expressions for the form factors [2]. For the $B \to D^*\mu\nu$ case, the three form factors are written as [2]

$$h_{A_1}(w) = h_{A_1}(1)[1 - 8\rho^2 z + (53\rho^2 - 15)z^2 - (231\rho^2 - 91)z^3], \quad (9)$$

$$R_1(w) = R_1(1) - 0.12(w-1) + 0.05(w-1)^2, \quad (10)$$

$$R_2(w) = R_2(1) - 0.11(w-1) - 0.06(w-1)^2, \quad (11)$$

where the same numerical coefficients, originally computed for B^0 decays, are considered also for B_s^0 decays, and where the conformal variable z is defined as

$$z \equiv \frac{\sqrt{w+1} - \sqrt{2}}{\sqrt{w+1} + \sqrt{2}}. \quad (12)$$

The form factors depend only on four parameters: ρ^2, $R_1(1)$, $R_2(1)$ and $h_{A_1}(1)$.

The BGL parametrization follows from more general arguments based on dispersion relations, analyticity, and crossing symmetry [3–5]. In the case of $B \to D^*\mu\nu$ decays, the form factors are written in terms of three functions, $f(w)$, $g(w)$ and $\mathcal{F}_1(w)$, as follows:

TABLE I. Functions describing the differential decay rate of $B \to D^*\mu\nu$ decays, separately for the cases in which the D^* meson decays to $D\gamma$ or $D\pi^0$.

		$k_i(\theta_\mu,\theta_D,\chi)$	
i	$\mathcal{H}_i(w)$	$D^* \to D\gamma$	$D^* \to D\pi^0$
1	H_+^2	$\frac{1}{2}(1+\cos^2\theta_D)(1-\cos\theta_\mu)^2$	$\sin^2\theta_D(1-\cos\theta_\mu)^2$
2	H_-^2	$\frac{1}{2}(1+\cos^2\theta_D)(1+\cos\theta_\mu)^2$	$\sin^2\theta_D(1+\cos\theta_\mu)^2$
3	H_0^2	$2\sin^2\theta_D\sin^2\theta_\mu$	$4\cos^2\theta_D\sin^2\theta_\mu$
4	H_+H_-	$\sin^2\theta_D\sin^2\theta_\mu\cos 2\chi$	$-2\sin^2\theta_D\sin^2\theta_\mu\cos 2\chi$
5	H_+H_0	$\sin 2\theta_D\sin\theta_\mu(1-\cos\theta_\mu)\cos\chi$	$-2\sin 2\theta_D\sin\theta_\mu(1-\cos\theta_\mu)\cos\chi$
6	H_-H_0	$-\sin 2\theta_D\sin\theta_\mu(1+\cos\theta_\mu)\cos\chi$	$2\sin 2\theta_D\sin\theta_\mu(1+\cos\theta_\mu)\cos\chi$

$$h_{A_1}(w) = \frac{f(w)}{\sqrt{m_B m_{D^*}}(1+w)}, \tag{13}$$

$$R_1(w) = (w+1) m_B m_{D^*} \frac{g(w)}{f(w)}, \tag{14}$$

$$R_2(w) = \frac{w-r}{w-1} - \frac{\mathcal{F}_1(w)}{m_B(w-1)f(w)}. \tag{15}$$

These functions are expanded as convergent power series of z as

$$f(z) = \frac{1}{P_{1^+}(z)\phi_f(z)} \sum_{n=0}^{\infty} b_n z^n, \tag{16}$$

$$g(z) = \frac{1}{P_{1^-}(z)\phi_g(z)} \sum_{n=0}^{\infty} a_n z^n, \tag{17}$$

$$\mathcal{F}_1(z) = \frac{1}{P_{1^+}(z)\phi_{\mathcal{F}_1}(z)} \sum_{n=0}^{\infty} c_n z^n. \tag{18}$$

Here, the $P_{1^\pm}(z)$ functions are known as Blaschke factors for the $J^P = 1^\pm$ resonances, and $\phi_{f,g,\mathcal{F}_1}(z)$ are the so-called outer functions. Adopting the formalism of Ref. [27], the Blaschke factors take the form

$$P_{1^\pm}(z) = C_{1^\pm} \prod_{k=1}^{\text{poles}} \frac{z - z_k}{1 - z z_k}, \tag{19}$$

where

$$z_k = \frac{\sqrt{t_+ - m_k^2} - \sqrt{t_+ - t_-}}{\sqrt{t_+ - m_k^2} + \sqrt{t_+ - t_-}}, \tag{20}$$

$t_\pm = (m_B \pm m_{D^*})^2$, and m_k denotes the pole masses of the kth excited B_c^+ states that are below the BD^* threshold and have the appropriate J^P quantum numbers. The constants $C_{1^\pm}$ are scale factors calculated to use in B_s^0 decays the same Blaschke factor derived for B^0 decays. The outer functions are defined as

$$\phi_f(z) = \frac{4r}{m_B^2} \sqrt{\frac{n_I}{3\pi\tilde{\chi}_{1^+}(0)}} \frac{(1+z)\sqrt{(1-z)^3}}{[(1+r)(1-z) + 2\sqrt{r}(1+z)]^4}, \tag{21}$$

$$\phi_g(z) = 16 r^2 \sqrt{\frac{n_I}{3\pi\tilde{\chi}_{1^-}(0)}} \times \frac{(1+z)^2}{\sqrt{(1-z)}[(1+r)(1-z) + 2\sqrt{r}(1+z)]^4}, \tag{22}$$

$$\phi_{\mathcal{F}_1}(z) = \frac{4r}{m_B^3} \sqrt{\frac{n_I}{6\pi\tilde{\chi}_{1^+}(0)}} \frac{(1+z)\sqrt{(1-z)^5}}{[(1+r)(1-z) + 2\sqrt{r}(1+z)]^5}, \tag{23}$$

TABLE II. Pole masses for the B_c^+ resonances considered in the BGL parameterization of the B_s^0 decays, with the $\tilde{\chi}_{J^P}(0)$ constants of the outer functions and the C_{J^P} constants of the Blaschke factors [8]. For B^0 decays, the Blaschke factors do not include the last 1^- resonance and $C_{1^\pm}$ both have unit value.

J^P	Pole mass [GeV/c^2]	$\tilde{\chi}_{J^P}(0)$ [10^{-4} GeV$^{-2}c^4$]	C_{J^P}
1^-	6.329	5.131	2.52733
	6.920		
	7.020		
	7.280		
1^+	6.739	3.894	2.02159
	6.750		
	7.145		
	7.150		

where $n_I = 2.6$ is the number of spectator quarks (three), corrected for $SU(3)$-breaking effects [8]. The B_c^+ resonances used in the computation of the Blaschke factors, the $\tilde{\chi}_{1^\pm}(0)$ coefficients of the outer functions, and the constants $C_{1^\pm}$ are reported in Table II. The coefficients of the series in Eqs. (16)–(18) are bound by the unitarity constraints

$$\sum_{n=0}^{\infty} a_n^2 \leq 1, \qquad \sum_{n=0}^{\infty} (b_n^2 + c_n^2) \leq 1. \tag{24}$$

The first coefficient of $f(z)$, b_0, is related to $h_{A_1}(1)$ by the expression

$$b_0 = 2\sqrt{m_B m_{D^*}} P_{1^+}(0)\phi_f(0) h_{A_1}(1), \tag{25}$$

while c_0 is fixed from b_0 through

$$c_0 = (m_B - m_{D^*}) \frac{\phi_{\mathcal{F}_1}(0)}{\phi_f(0)} b_0. \tag{26}$$

B. $B \to D\mu\nu$ decays

In the $B \to D\mu\nu$ case, the decay rate only depends upon the recoil variable $w = v_B \cdot v_D$. In the limit of negligible lepton masses, the differential decay rate can be written as [28]

$$\frac{\mathrm{d}\Gamma(B \to D\mu\nu)}{\mathrm{d}w} = \frac{G_F^2 m_D^3}{48\pi^3} (m_B + m_D)^2 \eta_{\mathrm{EW}}^2 \times |V_{cb}|^2 (w^2 - 1)^{3/2} |\mathcal{G}(w)|^2. \tag{27}$$

In the CLN parametrization, using the conformal variable $z(w)$ defined in Eq. (12), the form factor $\mathcal{G}(z)$ is expressed in terms of its value at zero recoil, $\mathcal{G}(0)$, and a slope parameter, ρ^2, as [2]

$$\mathcal{G}(z) = \mathcal{G}(0)[1 - 8\rho^2 z + (51\rho^2 - 10)z^2 - (252\rho^2 - 84)z^3]. \tag{28}$$

In the BGL parametrization, it is expressed as [3–5]

$$|\mathcal{G}(z)|^2 = \frac{4r}{(1+r)^2}|f_+(z)|^2, \tag{29}$$

with $r = m_D/m_B$ and

$$f_+(z) = \frac{1}{P_{1^-}(z)\phi(z)}\sum_{n=0}^{\infty} d_n z^n. \tag{30}$$

The outer function $\phi(z)$ is defined as

$$\phi(z) = \frac{8r^2}{m_B}\sqrt{\frac{8n_I}{3\pi\tilde{\chi}_{1^-}(0)}}\frac{(1+z)^2\sqrt{1-z}}{[(1+r)(1-z)+2\sqrt{r}(1+z)]^5}. \tag{31}$$

The coefficients of the series in Eq. (30) are bound by unitarity,

$$\sum_{n=0}^{\infty} d_n^2 \leq 1, \tag{32}$$

with the coefficient d_0 being related to $\mathcal{G}(0)$ through

$$d_0 = \frac{1+r}{2\sqrt{r}}\mathcal{G}(0)P_{1^-}(0)\phi(0). \tag{33}$$

III. DETECTOR AND SIMULATION

The LHCb detector [29,30] is a single-arm forward spectrometer covering the pseudorapidity range $2 < \eta < 5$, designed for the study of particles containing b or c quarks. The detector includes a high-precision tracking system consisting of a silicon-strip vertex detector surrounding the pp interaction region, a large-area silicon-strip detector located upstream of a dipole magnet with a bending power of about 4 Tm, and three stations of silicon-strip detectors and straw drift tubes placed downstream of the magnet. The tracking system provides a measurement of the momentum p of charged particles with a relative uncertainty that varies from 0.5% at low momentum to 1.0% at 200 GeV/c. The minimum distance of a track to a primary vertex, the impact parameter, is measured with a resolution of $(15 + 29/p_{\mathrm{T}})$ μm, where p_{T} is the component of the momentum transverse to the beam, in GeV/c. Different types of charged hadrons are distinguished using information from two ring-imaging Cherenkov detectors. Photons, electrons and hadrons are identified by a calorimeter system consisting of scintillating-pad and preshower detectors and an electromagnetic and a hadronic calorimeter. Muons are identified by a system composed of alternating layers of iron and multiwire proportional chambers.

Simulation is required to model the expected sample composition and develop the selection requirements, to calculate the reconstruction and selection efficiencies, and to build templates describing the distributions of signal and background decays used in the fit that determines the parameters of interest. In the simulation, pp collisions are generated using PYTHIA [31] with a specific LHCb configuration [32]. Decays of unstable particles are described by EvtGen [33], in which final-state radiation is generated using PHOTOS [34]. The interaction of the generated particles with the detector, and its response, are implemented using the GEANT4 toolkit [35] as described in Ref. [36]. The simulation is corrected for mismodeling of the reconstruction and selection efficiency, of the response of the particle identification algorithms, and of the kinematic properties of the generated $B^0_{(s)}$ mesons. The corrections are determined by comparing data and simulation in large samples of control decays, such as $D^{*+} \to D^0(\to K^-\pi^+)\pi^+$, $B^+ \to J/\psi(\to \mu^+\mu^-)K^+$, $B^0_s \to J/\psi(\to \mu^+\mu^-)\phi(\to K^+K^-)$, $B^0 \to D^-(\to K^+\pi^-\pi^-)\pi^+$, and $B^0_s \to D^-_s(\to K^+K^-\pi^-)\pi^+$. Residual small differences between data and the corrected simulation are accounted for in the systematic uncertainties.

IV. SELECTION AND EXPECTED SAMPLE COMPOSITION

The selection of the $B^0_{(s)} \to D^{(*)-}_{(s)}\mu^+\nu_\mu$ candidates closely follows that of Ref. [37]. Online, a trigger [38] selects events containing a high-p_{T} muon candidate associated with one, two, or three charged particles, all with origins displaced from the collision points. In the offline reconstruction, the muon candidate is combined with three charged particles consistent with the topology and kinematics of signal $B^0_s \to [K^+K^-\pi^-]_{D^-_s}\mu^+\nu_\mu$ and reference $B^0 \to [K^+K^-\pi^-]_{D^-}\mu^+\nu_\mu$ decays. The $K^+K^-\pi^-$ mass is restricted to be in the ranges $[1.945, 1.995]$ GeV/c^2 and $[1.850, 1.890]$ GeV/c^2 to define the inclusive samples of $D^-_s\mu^+$ signal and $D^-\mu^+$ reference candidates, respectively. Cross-contamination between signal and reference samples is smaller than 0.1%, as estimated from simulation. The K^+K^- mass must be in the range $[1.008, 1.032]$ GeV/c^2, to suppress the background under the $D^-_{(s)}$ peaks and ensure similar kinematic distributions for signal and reference decays. Same-sign $D^-_{(s)}\mu^-$ candidates are also reconstructed to model combinatorial background from accidental $D^-_{(s)}\mu^+$ associations. The candidate selection is optimized toward suppressing the background under the charm signals and making same-sign candidates a reliable model for the combinatorial background: track- and vertex-quality, vertex-displacement, transverse-momentum, and

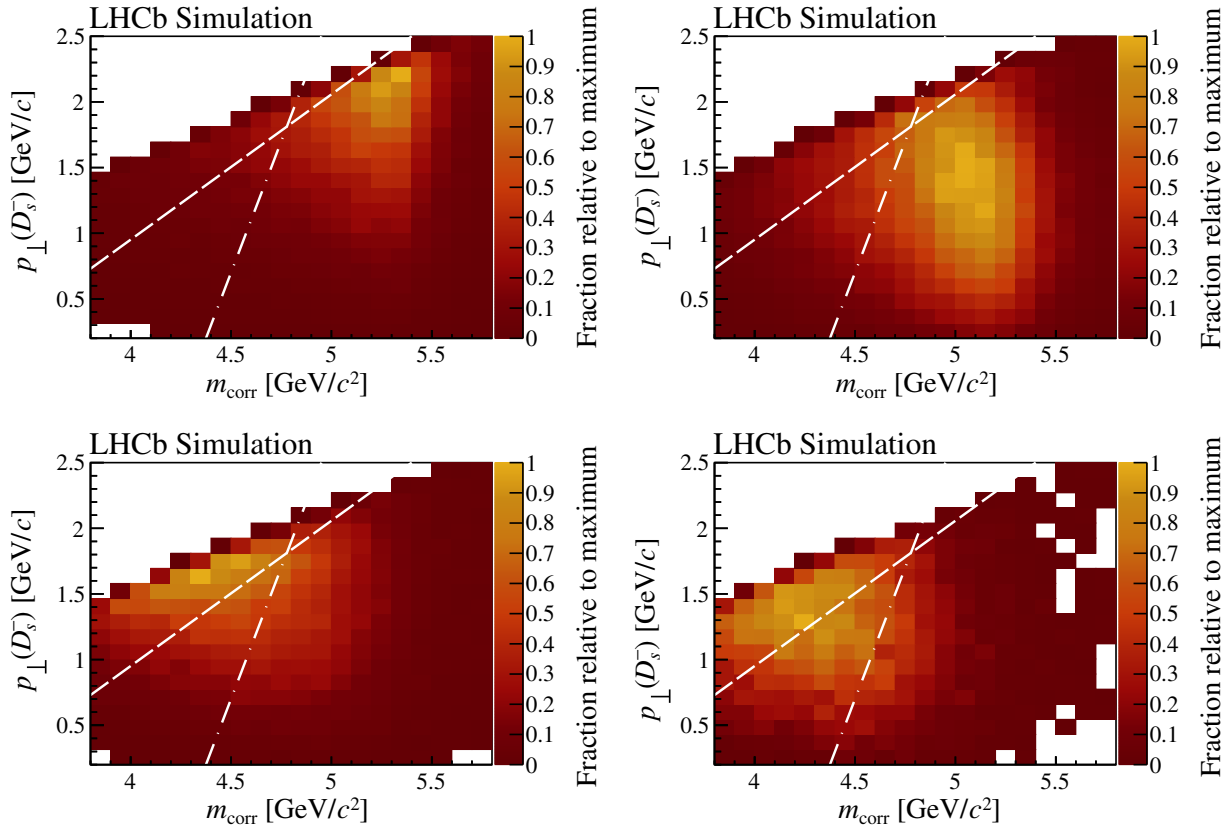

FIG. 2. Two-dimensional distributions of $p_\perp(D_s^-)$ versus $m_{\rm corr}$ for simulated (top left) $B_s^0 \to D_s^- \mu^+ \nu_\mu$ decays, (top right) $B_s^0 \to D_s^{*-} \mu^+ \nu_\mu$ decays, (bottom left) background decays from B_s^0 feed-down and b-hadron decays to a doubly charmed final state, and (bottom right) background decays from B^0 cross feed and semitauonic B_s^0 decays. The background components are grouped according to their shapes in the $m_{\rm corr}$ versus $p_\perp(D_s^-)$ space. The requirement $p_\perp(D_s^-)$ [GeV/c] $< 1.5 + 1.1 \times (m_{\rm corr}$ [GeV/c^2] $- 4.5)$ is drawn as a dashed line; the dot-dashed line shows the tighter requirement, applied on top of the baseline, which is used in Sec. VIII to further suppress background and assess the systematic uncertainty due to the residual contamination.

particle-identification criteria are chosen to minimize shape and yield differences between same-sign and signal candidates in the $m(D_{(s)}^- \mu^+) > 5.5$ GeV/c^2 region, where genuine b-hadron decays are kinematically excluded and combinatorial background dominates. Mass vetoes suppress to a negligible level background from misreconstructed decays, such as $B_s^0 \to \psi^{(\prime)}(\to \mu^+\mu^-)\phi(\to K^+K^-)$ decays where a muon is misidentified as a pion, $\Lambda_b^0 \to \Lambda_c^+(\to pK^-\pi^+)\mu^-\bar{\nu}_\mu X$ decays where the proton is misidentified as a kaon or a pion (and X indicates other possible final-state particles), and $B_{(s)}^0 \to D_{(s)}^- \pi^+$ decays where the pion is misidentified as a muon. The requirement $p_\perp(D_{(s)}^-)$ [GeV/c] $< 1.5 + 1.1 \times (m_{\rm corr}$ [GeV/c^2] $- 4.5)$ is imposed to suppress background from all other partially reconstructed b-hadron decays, as shown in Fig. 2 for B_s^0 decays. Tighter and looser variations of this requirement are used in Sec. VIII to estimate the systematic uncertainty due to the residual background contamination.

A total of 2.72×10^5 $D_s^- \mu^+$ and 0.82×10^5 $D^- \mu^+$ candidates satisfy the selection criteria. Simulation is used to describe all sources of b-hadron decays contributing to these inclusive samples. Assuming for $B_s^0 \to D_s^- \mu^+ \nu_\mu$ and $B_s^0 \to D_s^{*-} \mu^+ \nu_\mu$ decays the same branching fractions as for $B^0 \to D^- \mu^+ \nu_\mu$ and $B^0 \to D^{*-} \mu^+ \nu_\mu$, respectively, $B_s^0 \to D_s^- \mu^+ \nu_\mu$ and $B_s^0 \to D_s^{*-} \mu^+ \nu_\mu$ decays are expected to constitute about 30% and 60% of the inclusive sample of the selected $D_s^- \mu^+$ candidates, while $B^0 \to D^- \mu^+ \nu_\mu$ and $B^0 \to D^{*-} \mu^+ \nu_\mu$ decays are expected to constitute about 50% and 30% of the $D^- \mu^+$ sample. The lower expected fraction of semimuonic decays into $D_{(s)}^*$ mesons for B^0 decays compared to B_s^0 decays is due to the branching fraction of $D^{*-} \to D^- X$ decays. A significant background originates from $B_{(s)}^0$ semimuonic decays into excited $D_{(s)}^-$ states other than $D_{(s)}^{*-}$, indicated inclusively as $D_{(s)}^{**-}$ hereafter, or from decays with a nonresonant combination of a $D_{(s)}^{(*)-}$ with pions. All these decays are referred to as feed-down background in the following. The sum of all feed-down background sources from B^0 decays is expected to total about 9% of the $D^- \mu^+$ sample. For B_s^0 decays less experimental information is available to estimate the D_s^{**-} feed-down contamination to the $D_s^- \mu^+$ sample.

The decays considered here are those into $D^*_{s0}(2317)^-$ and $D_{s1}(2460)^-$ mesons, because these states have a mass below the kinematic threshold required to decay strongly into DK or D^*K final states. Decays into the $D_{s1}(2536)^-$ meson are also considered, even if this state is above the D^*K threshold, because it has been observed to decay to a D_s^- meson [39]. Branching fractions for these B_s^0 decays are not known, but, based on the yields measured in Ref. [37], they are estimated to be a few percent of the $D_s^-\mu^+$ sample. Background from semileptonic B^+ decays into a $D^-\mu^+X$ final state is expected to be about 9% of the $D^-\mu^+$ sample, including both semimuonic and semitauonic decays, with $\tau^+ \to \mu^+\nu_\mu\bar{\nu}_\tau$. Semitauonic $B^0_{(s)}$ decays are estimated to contribute less than 1% to both the $D_s^-\mu^+$ and $D^-\mu^+$ samples, comprising all decays into $D^{(*)-}_{(s)}$ mesons and their excited states. In the case of B_s^0 decays, as no experimental information is available, assumptions based on measurements of B^0 decays are made, and the same D_s^{**-} states considered for the semimuonic decays are included. Background can also originate from B^+, B^0, B_s^0 or Λ_b^0 decaying into a pair of charm hadrons, where one hadron is the fully reconstructed $D^-_{(s)}$ candidate and the other decays semileptonically. While this background is expected to be negligible in the $D^-\mu^+$ sample, it is estimated to be about 2% of the $D_s^-\mu^+$ sample, following Ref. [37]. Such decays include $B^0_{(s)} \to D^{(*)-}_{(s)}D^+_{(s)}$, $B^+ \to \bar{D}^{(*)0}D^{(*)+}$, $B_s^0 \to D^0D_s^-K^+$, $B_s^0 \to D^-D_s^+K^0$, $\Lambda_b^0 \to \Lambda_c^+D_s^{(*)-}X$, and $\Lambda_b^0 \to D_s^+\Lambda\mu^-\bar{\nu}_\mu X$. Cross-feed semileptonic B_s^0 decays can be neglected in the inclusive $D^-\mu^+$ sample, whereas those of B^0 and B^+ decays to final states with a D_s^- candidate and an unreconstructed kaon, such as $B \to D_s^{(*)-}K\mu^+\nu_\mu$, must be considered in the $D_s^-\mu^+$ sample. This contamination is estimated to be at most 2%.

Reconstruction and selection efficiencies are determined from simulation. Given that signal decays are measured relative to reference B^0 decays, only efficiency ratios are needed. They are measured to be 1.568 ± 0.008 for $B_s^0 \to D_s^-\mu^+\nu_\mu$ relative to $B^0 \to D^-\mu^+\nu_\mu$ decays and 1.464 ± 0.007 for $B_s^0 \to D_s^{*-}\mu^+\nu_\mu$ relative to $B^0 \to D^{*-}\mu^+\nu_\mu$ decays. They depart from unity mainly because of the requirement on $m(K^+K^-)$ to be around the $\phi(1020)$ mass. This requirement reduces systematic uncertainties due to the modeling of trigger and particle-identification criteria. However, its efficiency relies on an accurate description in the simulation of the $D^-_{(s)} \to K^+K^-\pi^-$ amplitude model; a systematic uncertainty is assigned to cover for a possible mismodeling, as discussed in Sec. VIII. An additional difference between the efficiency of signal and reference decays originates from the D^- lifetime being about 2 times longer than the D_s^- lifetime [39]. The trigger selection is more efficient for decays with closely spaced $B^0_{(s)}$ and $D^-_{(s)}$ vertices, favoring smaller $D^-_{(s)}$ flight distances and hence decay times [37]. As a consequence, the efficiency for selecting $D_s^-\mu^+$ candidates in the trigger is about 10% larger than that for $D^-\mu^+$ candidates.

V. ANALYSIS METHOD

Signal and reference yields can be precisely measured through a fit to the corrected mass distribution following the method of Ref. [37]. To be able to access the form factors, yields are measured as a function of the recoil variable w and of the helicity angles, as discussed in Sec. II. However, these quantities cannot be computed precisely because of the undetected neutrino and the inability to resolve the b-hadron kinematic properties by balancing it against the accompanying $\bar{b}$ hadron produced in the event, as done in e^+e^- collisions.

Approximate methods, based on geometric and kinematic constraints and on the assumption that only the neutrino is undetected, allow the determination of these quantities up to a twofold ambiguity in the neutrino momentum component parallel to the b-hadron flight direction [40–43]. Such an ambiguity can be resolved, e.g., by using multivariate regression algorithms [44] or by imposing additional constraints on the b-hadron production [45]. These approximate methods have already been successfully used by several LHCb analyses of semileptonic b-hadron decays [46–49]. However, $\mathcal{O}(20\%)$ inefficiencies are introduced because, due to resolution effects, the second-order equation responsible for the twofold ambiguity does not always have real solutions. The inability to use candidates for which no real solutions are found also restricts the candidate $m_{\rm corr}$ values to be smaller than the nominal $B^0_{(s)}$ mass, thus reducing the discriminating power between the different sample components.

To overcome such problems, a novel approach is adopted in this analysis. In $B^0_{(s)} \to D^-_{(s)}\mu^+\nu_\mu$ decays the component of the $D^-_{(s)}$ momentum perpendicular to the $B^0_{(s)}$ flight direction, $p_\perp(D^-_{(s)})$, is opposite and equal in magnitude to the component of the W^+ momentum vector that is perpendicular to the $B^0_{(s)}$ flight direction. Therefore, $p_\perp(D^-_{(s)})$ is highly correlated with w, as shown in the top-left distribution of Fig. 3 for B_s^0 decays. In $B^0_{(s)} \to D^{*-}_{(s)}\mu^+\nu_\mu$ decays the correlation is kept, as shown in the top-right distribution of Fig. 3, because the unreconstructed photon or pion from the $D^{*-}_{(s)}$ decay carries very little energy, which only leads to a small dilution. In these decays, the $p_\perp(D^-_{(s)})$ variable is also correlated, albeit to a lesser extent, with the helicity angles θ_μ and θ_D, as shown in the bottom distributions of Fig. 3 for B_s^0 decays. Through such correlations, the distribution of $p_\perp(D^-_{(s)})$ has a strong dependence on the form factors, particularly on $\mathcal{G}(w)$ for the scalar case and on $h_{A_1}(w)$ for the vector case.

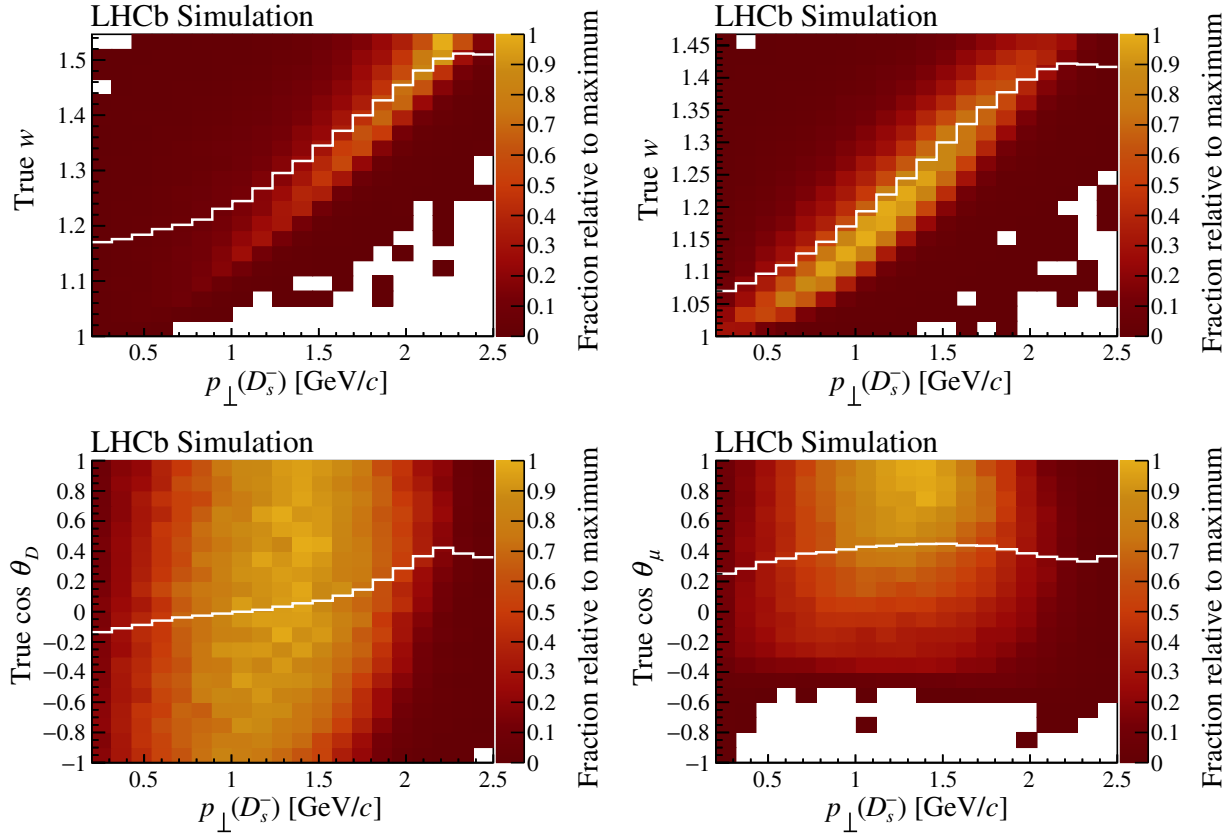

FIG. 3. (Top) Distribution of true value of the w recoil variable versus reconstructed $p_\perp(D_s^-)$ for (left) $B_s^0 \to D_s^- \mu^+ \nu_\mu$ and (right) $B_s^0 \to D_s^{*-} \mu^+ \nu_\mu$ simulated decays. (Bottom) Distribution of the true values of (left) $\cos\theta_D$ and (right) $\cos\theta_\mu$ versus reconstructed $p_\perp(D_s^-)$ for $B_s^0 \to D_s^{*-} \mu^+ \nu_\mu$ simulated decays. Only simulated candidates that fulfill the selection requirements are shown. In each histogram the solid line represents the average of the variable displayed on the vertical axis as a function of $p_\perp(D_s^-)$. The distributions of $B^0 \to D^{*-} \mu^+ \nu_\mu$ decays show similar features.

Therefore, the form factors can be accessed by analysing the shape of the $p_\perp(D_{(s)}^-)$ distribution of the signal decays, with no need to estimate the momentum of the unreconstructed particles. The $p_\perp(D_{(s)}^-)$ variable has the experimental advantage of being reconstructed fully from the tracks of the $D_{(s)}^-$ decay products and from the well-measured origin and decay vertices of the $B_{(s)}^0$ meson. It is also correlated with $m_{\rm corr}$, and the two variables together provide very efficient discrimination between signal and background decays, which accumulate in different regions of the two-dimensional space spanned by $m_{\rm corr}$ and $p_\perp(D_{(s)}^-)$, as already shown in Fig. 2 for B_s^0 decays.

A least-squares fit to the $m_{\rm corr}$-$p_\perp(D_{(s)}^-)$ distribution of the selected inclusive samples of $D_{(s)}^- \mu^+$ candidates is used to simultaneously determine the form factors and (signal) reference yields that are needed for the measurement of $|V_{cb}|$ or of the ratios of branching fractions $\mathcal{R}^{(*)}$. In the fit, the data are described by several fit components, which will be detailed later, separately for the B^0 and B_s^0 cases. The shape of each component in the $m_{\rm corr}$-$p_\perp(D_{(s)}^-)$ space is modeled with two-dimensional histogram templates derived either from simulation (for signal, reference and all physics background decays) or from same-sign data candidates (for combinatorial background). The binning of the histograms is chosen such that there are at least 15 entries per bin (for both data and templates distributions), to guarantee unbiased estimates of the least-squares fit. A few bins at the edges of the $m_{\rm corr}$-$p_\perp(D_{(s)}^-)$ space have a smaller number of entries, but studies performed on pseudoexperiments show that they do not introduce biases in the fit results.

Signal templates are built using a per-candidate weight calculated as the ratio between the differential decay rate featuring a given set of form-factor parameters and that with the parameters used in the generation of the simulated samples. The set of parameters of the differential decay rate at the numerator is varied in the least-squares minimization. The differential decay rates are given in Eq. (4) for $B_{(s)}^0 \to D_{(s)}^{*-} \mu^+ \nu_\mu$ decays and in Eq. (27) for $B_{(s)}^0 \to D_{(s)}^- \mu^+ \nu_\mu$ decays. They are evaluated at the candidate true value of w and of the helicity angles for $B_{(s)}^0 \to D_{(s)}^{*-} \mu^+ \nu_\mu$. The $m_{\rm corr}$-$p_\perp(D_{(s)}^-)$ templates are rebuilt at each iteration of the least-squares minimization using the values of

form-factor parameters probed at that iteration. With this weighting procedure, all efficiency and resolution effects are accounted for, making the templates independent of the form-factor values assumed in the generation of the simulated candidates.

In the fit, the yield of each component is a free parameter. To determine $|V_{cb}|$, the signal yields $N_{\rm sig}^{(*)}$ are expressed as the integral of the differential decay rates multiplied by the B_s^0 lifetime τ. The signal yields are normalized to the yields $N_{\rm ref}^{(*)}$ and to the measured branching fractions of the reference B^0 modes, correcting for the efficiency ratios between signal and reference decays, $\xi^{(*)}$. The full expression for the signal yields is

$$N_{\rm sig}^{(*)} = \mathcal{N}^{(*)}\tau \int \frac{{\rm d}\Gamma(B_s^0 \to D_s^{(*)-}\mu^+\nu_\mu)}{{\rm d}\zeta}{\rm d}\zeta, \qquad (34)$$

where the integral is performed over $\zeta \equiv w$ for $B_s^0 \to D_s^-\mu^+\nu_\mu$ and $\zeta \equiv (w, \cos\theta_\mu, \cos\theta_D, \chi)$ for $B_s^0 \to D_s^{*-}\mu^+\nu_\mu$ and where

$$\mathcal{N}^{(*)} \equiv \frac{N_{\rm ref}^{(*)}\xi^{(*)}\mathcal{K}^{(*)}}{\mathcal{B}(B^0 \to D^{(*)-}\mu^+\nu_\mu)}, \qquad (35)$$

$$\mathcal{K} \equiv \frac{f_s}{f_d}\frac{\mathcal{B}(D_s^- \to K^+K^-\pi^-)}{\mathcal{B}(D^- \to K^+K^-\pi^-)}, \qquad (36)$$

$$\mathcal{K}^* \equiv \frac{f_s}{f_d}\frac{\mathcal{B}(D_s^- \to K^+K^-\pi^-)}{\mathcal{B}(D^{*-} \to D^-X)\mathcal{B}(D^- \to K^+K^-\pi^-)}, \qquad (37)$$

with f_s/f_d being the ratio of B_s^0- to B^0-meson production fractions. The dependence on $|V_{cb}|$ in Eq. (34) is enclosed in the differential decay rate of Eqs. (4) and (27). The other parameters entering the differential decay rate are either left free to float in the fit, together with $|V_{cb}|$, or constrained to external determinations by a penalty term in the least-squares function, as detailed in the following sections. A similar fit is performed to determine the ratios of branching fractions, with the difference that the expression of the signal yields simplifies to

$$N_{\rm sig}^{(*)} = N_{\rm ref}^{(*)}\xi^{(*)}\mathcal{K}^{(*)}\mathcal{R}^{(*)}, \qquad (38)$$

and $\mathcal{R}$ and $\mathcal{R}^*$ become free parameters instead of $|V_{cb}|$. In the fit to the reference sample, the yields are free parameters, not expressed in terms of $|V_{cb}|$. Their histogram templates are functions of the form factors and are allowed to float in the fit.

VI. FIT TO THE REFERENCE SAMPLE

The reference yields $N_{\rm ref}^{(*)}$ are determined by fitting the $m_{\rm corr}$-$p_\perp(D^-)$ distribution of the inclusive $D^-\mu^+$ sample using the following four components: the two reference decays $B^0 \to D^-\mu^+\nu_\mu$ and $B^0 \to D^{*-}\mu^+\nu_\mu$; physics background due to the sum of semileptonic B^0 feed-down and $B^+ \to D^-\mu^+X$ decays; and combinatorial background. The $B^0 \to D^{*-}\mu^+\nu_\mu$ template is generated assuming a fraction of approximately 5% for $D^{*-} \to D^-\gamma$ decays and 95% for $D^{*-} \to D^-\pi^0$ decays, according to the measured D^{*-} branching fractions [39]. The physics background components are grouped together into a single template because their $m_{\rm corr}$-$p_\perp(D^-)$ distributions are too similar to be discriminated by the fit. A contribution from semitauonic decays is neglected because its yield is found to be consistent with zero in an alternate fit in which this component is included, and no significant change of the reference yields is observed. The fit parameters are $N_{\rm ref}^{(*)}$, the yields of the background components and the $B^0 \to D^{(*)-}\mu^+\nu_\mu$ form-factor parameters expressed in the CLN parametrization: $\rho^2(D^-)$, $\rho^2(D^{*-})$, $R_1(1)$ and $R_2(1)$. Given the limited size of the $D^-\mu^+$ samples, the CLN

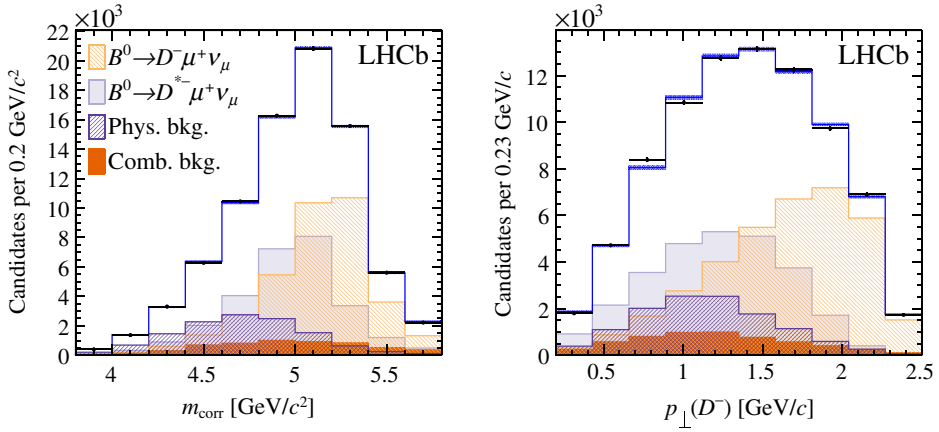

FIG. 4. Distribution of (left) $m_{\rm corr}$ and (right) $p_\perp(D^-)$ for the inclusive sample of reference $D^-\mu^+$ candidates, with fit projections overlaid.

parametrization is preferred over BGL because of its reduced number of free parameters.

The reference yields are determined to be $N_{\rm ref} = (36.4 \pm 1.6) \times 10^3$ and $N^*_{\rm ref} = (27.8 \pm 1.2) \times 10^3$ with a correlation of -70.3%. These results do not depend significantly on the choice of the form-factor parametrization. The one-dimensional projections of the fit on the $m_{\rm corr}$ and $p_\perp(D^-)$ variables are shown in Fig. 4. The fit describes the data well with a minimum χ^2/ndf of 76/70, corresponding to a p value of 29%. The form-factor parameters are measured to be in agreement with their world-average values [1], with relative uncertainties ranging from 20% to 50% depending on the parameter.

VII. FIT TO THE SIGNAL SAMPLE

The fit function for the $D_s^-\mu^+$ sample features five components: the two signal decays $B_s^0 \to D_s^-\mu^+\nu_\mu$ and $B_s^0 \to D_s^{*-}\mu^+\nu_\mu$; a background component made by the sum of semimuonic B_s^0 feed-down decays and b-hadron decays to a doubly charmed final state; a background component made by the sum of cross-feed semileptonic B^0 decays and semitauonic B_s^0 decays; and combinatorial background. The $B_s^0 \to D_s^{*-}\mu^+\nu_\mu$ template is generated assuming a fraction of approximately 94% for $D_s^{*-} \to D_s^-\gamma$ decays and 6% for $D_s^{*-} \to D_s^-\pi^0$ decays, according to the measured D_s^{*-} branching fractions [39]. The physics background components that are merged together in the two templates have very similar shapes in the $m_{\rm corr}$ versus $p_\perp(D_s^-)$ plane and cannot be discriminated by the fit when considered as separate components. They are therefore merged according to the expected approximate fractions.

The yields of the five components are free parameters in the fit, with the signal yields expressed in terms of the parameters of interest according to Eq. (34), when determining $|V_{cb}|$, or Eq. (38), when determining $\mathcal{R}^{(*)}$. The measurement relies on the external inputs reported in Tables III and IV. Correlations between external inputs, e.g., between $N_{\rm ref}$ and $N^*_{\rm ref}$ or between the LQCD inputs, are accounted for in the fit. The value of f_s/f_d is derived from the measurement of Ref. [24], which is the most precise available. It is obtained using an independent sample of semileptonic $B^0_{(s)}$ decays collected with the LHCb detector in pp collisions at the center-of-mass energy of 13 TeV. This measurement uses the branching fraction of the $D_s^- \to K^+K^-\pi^-$ decay and the B_s^0 lifetime as external inputs [39]. To properly account for all correlations, the value of the product $f_s/f_d \times \mathcal{B}(D_s^- \to K^-K^+\pi^-) \times \tau$ is derived directly from Ref. [24]. The measured dependence of f_s/f_d on the collision energy [50] is also accounted for in the computation, by scaling the 13 TeV measurement to the value at 7 and 8 TeV needed in this analysis. All other branching fractions and the particle masses are taken from Ref. [39]. The external inputs listed in Table IV are based exclusively on theory calculations: $\eta_{\rm EW}$ and $h_{A_1}(1)$ are constrained to the values reported in Refs. [26,18], respectively; the constraints on the $B_s^0 \to D_s^-\mu^+\nu_\mu$ form factors are based on the LQCD calculations of Ref. [23], which provide the form factor $f_+(z)$ over the full q^2 spectrum using the parametrization proposed by Bourrely, Caprini and Lellouch (BCL) [6]. In Appendix A, the corresponding CLN and BGL parameters reported in Table IV are derived.

TABLE III. External inputs based on experimental measurements.

Parameter	Value	Reference
$f_s/f_d \times \mathcal{B}(D_s^- \to K^-K^+\pi^-) \times \tau$ [ps]	0.0191 ± 0.0008	[24,50]
$\mathcal{B}(D^- \to K^-K^+\pi^-)$	0.00993 ± 0.00024	[39]
$\mathcal{B}(D^{*-} \to D^-X)$	0.323 ± 0.006	[39]
$\mathcal{B}(B^0 \to D^-\mu^+\nu_\mu)$	0.0231 ± 0.0010	[39]
$\mathcal{B}(B^0 \to D^{*-}\mu^+\nu_\mu)$	0.0505 ± 0.0014	[39]
B_s^0 mass [GeV/c^2]	5.36688 ± 0.00017	[39]
D_s^- mass [GeV/c^2]	1.96834 ± 0.00007	[39]
D_s^{*-} mass [GeV/c^2]	2.1122 ± 0.0004	[39]

TABLE IV. External inputs based on theory calculations. The values and their correlations are derived in Appendix A, based on Ref. [23].

Parameter	Value	Reference
$\eta_{\rm EW}$	1.0066 ± 0.0050	[26]
$h_{A_1}(1)$	0.902 ± 0.013	[18]
CLN parametrization		
$\mathcal{G}(0)$	1.07 ± 0.04	[23]
$\rho^2(D_s^-)$	1.23 ± 0.05	[23]
BGL parametrization		
$\mathcal{G}(0)$	1.07 ± 0.04	[23]
d_1	-0.012 ± 0.008	[23]
d_2	-0.24 ± 0.05	[23]

A. Determination of $|V_{cb}|$ with the CLN parametrization

The analysis in the CLN parametrization uses the form factors defined in Eqs. (9)–(11), for $B_s^0 \to D_s^{*-}\mu^+\nu_\mu$ decays, and in Eq. (28), for $B_s^0 \to D_s^-\mu^+\nu_\mu$ decays. The form-factor parameters $\rho^2(D_s^{*-})$, $R_1(1)$, and $R_2(1)$ are free to float in the fit, while $h_{A_1}(1)$, $\mathcal{G}(0)$ and $\rho^2(D_s^-)$ are constrained.

One-dimensional projections of the fit results on $m_{\rm corr}$ and $p_\perp(D_s^-)$ are shown in Fig. 5. The fit has a minimum χ^2/ndf of 279/285, corresponding to a p value of 58%. The results for the parameters of interest are reported in Table V. In addition to $|V_{cb}|$, these include the form-factor parameters that are determined exclusively by the data,

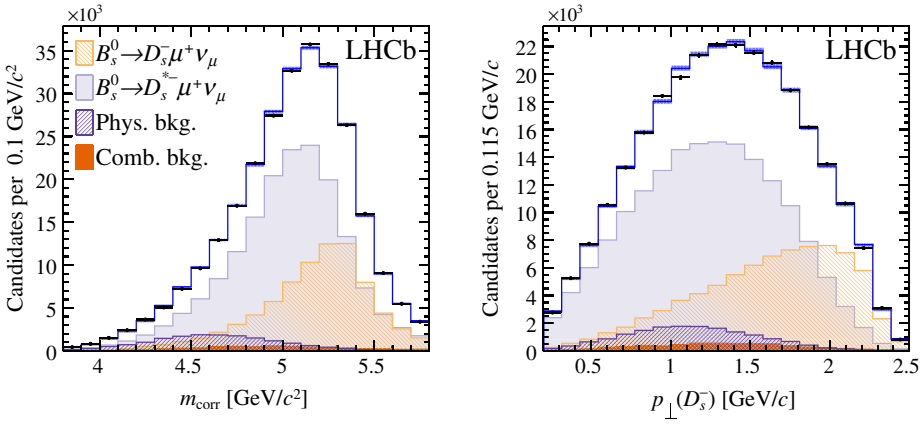

FIG. 5. Distribution of (left) $m_{\rm corr}$ and (right) $p_\perp(D_s^-)$ for the inclusive sample of signal $D_s^- \mu^+$ candidates, with fit projections based on the CLN parametrization overlaid. The projections of the two physics background components are merged together for displaying purposes.

such as $\rho^2(D_s^{*-})$, $R_1(1)$ and $R_2(1)$, and those for which the precision improves compared to the external constraints, such as $\mathcal{G}(0)$ and $\rho^2(D_s^-)$. Detailed fit results for all parameters, including their correlations, are reported in Appendix B. The uncertainties returned by the fit include the statistical contribution arising from the limited size of the data and simulation samples (stat) and the contribution due to the external inputs (ext). The calculation of this latter contribution is detailed in Sec. VIII. The value of $|V_{cb}|$, $(41.4 \pm 0.6(\text{stat}) \pm 1.2(\text{ext})) \times 10^{-3}$, agrees with the exclusive determination from B^+ and B^0 decays [1]. When only $\mathcal{G}(0)$ is constrained and $\rho^2(D_s^-)$ is left free, the fit returns $\rho^2(D_s^-) = 1.30 \pm 0.06(\text{stat})$, in agreement with the LQCD estimation, and $|V_{cb}| = (41.8 \pm 0.8(\text{stat}) \pm 1.2(\text{ext})) \times 10^{-3}$. Including the constraint on $\rho^2(D_s^-)$ improves the statistical precision on $|V_{cb}|$ by about 20% and also that on $\mathcal{G}(0)$ by 10%, because of the large correlation between $\mathcal{G}(0)$ and $\rho^2(D_s^-)$.

B. Determination of $|V_{cb}|$ with the BGL parametrization

The BGL form-factor functions are given by Eqs. (13)–(15), for $B_s^0 \to D_s^{*-} \mu^+ \nu_\mu$ decays, and Eq. (30), for $B_s^0 \to D_s^- \mu^+ \nu_\mu$ decays. The fit parameters are the coefficients of the series of the z expansion. For $B_s^0 \to D_s^{*-} \mu^+ \nu_\mu$ decays, the expansion of the f, g and $\mathcal{F}_1$ form factors is truncated after the first order in z. The coefficients b_0 and c_0 are constrained through $h_{A_1}(1)$ using Eqs. (25) and (26). The coefficients b_1, a_0, a_1, and c_1 are free parameters. For $B_s^0 \to D_s^- \mu^+ \nu_\mu$ decays, the expansion of the $f_+(z)$ form factor is truncated after the second order in z and the coefficients d_0, d_1 and d_2 are constrained to the values obtained in Appendix A using Ref. [23], with d_0 expressed in terms of the parameter $\mathcal{G}(0)$ using Eq. (33). No constraints from the unitarity bounds of Eqs. (24) and (32) are imposed, to avoid potential biases on the parameters or fit instabilities due to convergence at the boundary of the parameter space.

TABLE V. Fit results in the CLN parametrization. The uncertainty is split into two contributions, statistical (stat) and that due to the external inputs (ext).

Parameter	Value
$\lvert V_{cb}\rvert$ $[10^{-3}]$	$41.4 \pm 0.6(\text{stat}) \pm 1.2(\text{ext})$
$\mathcal{G}(0)$	$1.102 \pm 0.034(\text{stat}) \pm 0.004(\text{ext})$
$\rho^2(D_s^-)$	$1.27 \pm 0.05(\text{stat}) \pm 0.00(\text{ext})$
$\rho^2(D_s^{*-})$	$1.23 \pm 0.17(\text{stat}) \pm 0.01(\text{ext})$
$R_1(1)$	$1.34 \pm 0.25(\text{stat}) \pm 0.02(\text{ext})$
$R_2(1)$	$0.83 \pm 0.16(\text{stat}) \pm 0.01(\text{ext})$

The fit has minimum χ^2/ndf of 276/284, corresponding to a p value of 63%. Figure 6 shows a comparison of the $p_\perp(D_s^-)$ background-subtracted distributions obtained with the CLN and BGL fits. No significant differences are found between the two fits for both $B_s^0 \to D_s^- \mu^+ \nu_\mu$ and $B_s^0 \to D_s^{*-} \mu^+ \nu_\mu$ decays. The fit results for the parameters of interest are reported in Table VI. Detailed fit results for all parameters, including their correlations, are reported in Appendix B. The values found for the form-factor coefficients satisfy the unitarity bounds of Eqs. (24) and (32). The value of $|V_{cb}|$ is found to be $(42.3 \pm 0.8(\text{stat}) \pm 1.2(\text{ext})) \times 10^{-3}$, in agreement with the CLN analysis. The correlation between the BGL and CLN results is 34.0%. When only $\mathcal{G}(0)$ is constrained and d_1 and d_2 are left free, $|V_{cb}|$ is found to be $(42.2 \pm 1.5(\text{stat}) \pm 1.2(\text{ext})) \times 10^{-3}$. The constraints on d_1 and d_2 improve the statistical precision on $|V_{cb}|$ by about 50% and that on $\mathcal{G}(0)$ by 10%. Without such constraints, the fit returns $d_1 = 0.02 \pm 0.05(\text{stat})$ and $d_2 = -0.9 \pm 0.8(\text{stat})$, both in agreement with the LQCD estimations and within the unitarity bound of Eq. (32).

Variations of the orders of the form-factor expansions have been probed for the $B_s^0 \to D_s^{*-} \mu^+ \nu_\mu$ decay, while for

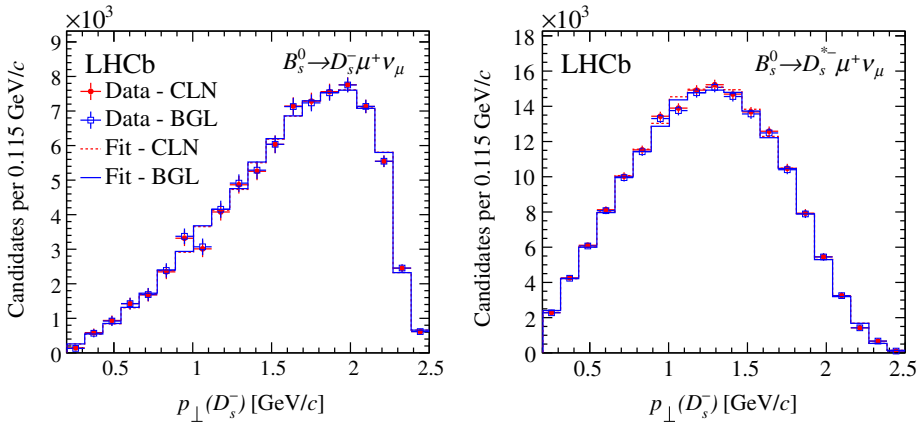

FIG. 6. Background-subtracted distribution of $p_\perp(D_s^-)$ for (left) $B_s^0 \to D_s^- \mu^+ \nu_\mu$ and (right) $B_s^0 \to D_s^{*-} \mu^+ \nu_\mu$ decays obtained from the fit based on the (red closed points, dashed line) CLN and (blue open points, solid line) BGL parametrizations, with corresponding fit projections overlaid.

the $B_s^0 \to D_s^- \mu^+ \nu_\mu$ decay the expansion is kept at order z^2 to exploit the constraints on d_1 and d_2. A first alternative fit, where only the order zero of the g series is considered by fixing a_1 to zero, returns a p value of 62% and $|V_{cb}| = (41.7 \pm 0.6(\text{ext}) \pm 1.2(\text{ext})) \times 10^{-3}$, in agreement with the nominal result of Table VI. The shift in the central value of $|V_{cb}|$ is consistent with that observed in pseudoexperiments where data are generated by using the nominal truncation and fit with the zero-order expansion of g. In a second alternative fit, g is kept at order zero and f is expanded at order z^2, by adding the coefficient b_2 as a free parameter. The fit has a p value of 64% and returns $|V_{cb}| = (42.2 \pm 0.8(\text{stat}) \pm 1.2(\text{ext})) \times 10^{-3}$ and $b_2 = 1.9 \pm 1.4(\text{stat})$. Configurations at lower order than those considered for f and $\mathcal{F}_1$ lead to poor fit quality and are discarded. Higher orders than those discussed here are not considered because they result in fit instabilities and degrade the sensitivity to $|V_{cb}|$ and to the form-factor coefficients.

C. Determination of $\mathcal{R}$ and $\mathcal{R}^*$

The ratios of B_s^0 to B^0 branching fractions are determined by a fit where the signal yields are expressed using Eq. (38), with $\mathcal{R}$ and $\mathcal{R}^*$ as free parameters. In the fit, the constraint on $f_s/f_d \times \mathcal{B}(D_s^- \to K^+K^-\pi^-)$ is obtained by dividing the value of the first row of Table III by the B_s^0 lifetime τ [39]. The form factors are expressed in the CLN parametrization and a systematic uncertainty is assigned for this arbitrary choice, as discussed in Sec. VIII. The fit returns $\mathcal{R} = 1.09 \pm 0.05(\text{stat}) \pm 0.05(\text{ext})$ and $\mathcal{R}^* = 1.06 \pm 0.05(\text{stat}) \pm 0.05(\text{ext})$, with a p value of 59%. Detailed fit results for all fit parameters, including their correlations, are reported in Appendix B.

TABLE VI. Fit results in the BGL parametrization. The uncertainty is split into two contributions, statistical (stat) and that due to the uncertainty on the external inputs (ext).

Parameter	Value
$\lvert V_{cb}\rvert$ $[10^{-3}]$	$42.3 \pm 0.8(\text{stat}) \pm 1.2(\text{ext})$
$\mathcal{G}(0)$	$1.097 \pm 0.034(\text{stat}) \pm 0.001(\text{ext})$
d_1	$-0.017 \pm 0.007(\text{stat}) \pm 0.001(\text{ext})$
d_2	$-0.26 \pm 0.05(\text{stat}) \pm 0.00(\text{ext})$
b_1	$-0.06 \pm 0.07(\text{stat}) \pm 0.01(\text{ext})$
a_0	$0.037 \pm 0.009(\text{stat}) \pm 0.001(\text{ext})$
a_1	$0.28 \pm 0.26(\text{stat}) \pm 0.08(\text{ext})$
c_1	$0.0031 \pm 0.0022(\text{stat}) \pm 0.0006(\text{ext})$

VIII. SYSTEMATIC UNCERTAINTIES

Systematic uncertainties affecting the measurements can be split into two main categories: those due to external inputs, indicated with (ext), and those due to the experimental methods, indicated with (syst). The individual contributions for each category are discussed in the following and are reported in Table VII, together with the statistical uncertainties.

The uncertainties returned by the fit include the statistical contribution arising from the finite size of the data and simulation samples and the contribution due to the external inputs that constrain some of the fit parameters through penalty terms in the least-squares function. To evaluate the purely statistical component, a second fit is performed with all external parameters fixed to the values determined by the first fit. The contribution due to the external inputs is then obtained by subtracting in quadrature the uncertainties from the two sets of results. The procedure is repeated for each individual input to estimate its contribution to the uncertainty. The results are reported in the upper section of Table VII. Here the uncertainty on $f_s/f_d \times \mathcal{B}(D_s^- \to K^+K^-\pi^-)(\times\tau)$ comprises also that due to a difference in the distribution of the transverse momentum of the $D_{(s)}^- \mu^+$ system with respect to Ref. [24], which results in a relative 1% change of the value of f_s/f_d. The branching fractions

TABLE VII. Summary of the uncertainties affecting the measured parameters. The upper section reports the systematic uncertainties due to the external inputs (ext), the middle section those due to the experimental methods (syst), and the lower section the statistical uncertainties (stat). For the first source of uncertainty the multiplication by τ holds only for the $|V_{cb}|$ fits.

	Uncertainty															
	CLN parametrization						BGL parametrization									
Source	$\lvert V_{cb}\rvert$ $[10^{-3}]$	$\rho^2(D_s^-)$ $[10^{-1}]$	$\mathcal{G}(0)$ $[10^{-2}]$	$\rho^2(D_s^{*-})$ $[10^{-1}]$	$R_1(1)$ $[10^{-1}]$	$R_2(1)$ $[10^{-1}]$	$\lvert V_{cb}\rvert$ $[10^{-3}]$	d_1 $[10^{-2}]$	d_2 $[10^{-1}]$	$\mathcal{G}(0)$ $[10^{-2}]$	b_1 $[10^{-1}]$	c_1 $[10^{-3}]$	a_0 $[10^{-2}]$	a_1 $[10^{-1}]$	$\mathcal{R}$ $[10^{-1}]$	$\mathcal{R}^*$ $[10^{-1}]$
$f_s/f_d \times \mathcal{B}(D_s^- \to K^+K^-\pi^-)(\times\tau)$	0.8	0.0	0.0	0.0	0.0	0.0	0.8	0.0	0.0	0.0	0.0	0.0	0.0	0.1	0.4	0.4
$\mathcal{B}(D^- \to K^-K^+\pi^-)$	0.5	0.0	0.0	0.0	0.0	0.0	0.5	0.0	0.0	0.0	0.0	0.0	0.0	0.1	0.3	0.3
$\mathcal{B}(D^{*-} \to D^-X)$	0.2	0.0	0.1	0.0	0.1	0.0	0.1	0.0	0.0	0.1	0.0	0.2	0.0	0.3	…	0.2
$\mathcal{B}(B^0 \to D^-\mu^+\nu_\mu)$	0.4	0.0	0.3	0.1	0.2	0.1	0.5	0.1	0.0	0.1	0.1	0.4	0.1	0.7	…	…
$\mathcal{B}(B^0 \to D^{*-}\mu^+\nu_\mu)$	0.3	0.0	0.2	0.1	0.1	0.1	0.2	0.0	0.0	0.1	0.1	0.3	0.1	0.4	…	…
$m(B_s^0)$, $m(D^{(*)-})$	0.0	0.0	0.0	0.0	0.0	0.0	0.0	0.0	0.0	0.0	0.0	0.0	0.0	0.1	…	…
η_{EW}	0.2	0.0	0.0	0.0	0.0	0.0	0.2	0.0	0.0	0.0	0.0	0.0	0.0	0.1	…	…
$h_{A_1}(1)$	0.3	0.0	0.2	0.1	0.1	0.1	0.3	0.0	0.0	0.1	0.1	0.3	0.1	0.5	…	…
External inputs (ext)	1.2	0.0	0.4	0.1	0.2	0.1	1.2	0.1	0.0	0.1	0.1	0.6	0.1	0.8	0.5	0.5
$D_{(s)}^- \to K^+K^-\pi^-$ model	0.8	0.0	0.0	0.0	0.0	0.0	0.8	0.0	0.0	0.0	0.0	0.0	0.0	0.0	0.5	0.4
Background	0.4	0.3	2.2	0.5	0.9	0.7	0.1	0.5	0.2	2.3	0.7	2.0	0.5	2.0	0.4	0.6
Fit bias	0.0	0.0	0.0	0.0	0.0	0.0	0.2	0.0	0.0	0.0	0.2	0.4	0.2	0.4	0.0	0.0
Corrections to simulation	0.0	0.0	0.5	0.0	0.1	0.0	0.0	0.1	0.0	0.1	0.0	0.0	0.0	0.1	0.0	0.0
Form-factor parametrization	…	…	…	…	…	…	…	…	…	…	…	…	…	…	0.0	0.1
Experimental (syst)	0.9	0.3	2.2	0.5	0.9	0.7	0.9	0.5	0.2	2.3	0.7	2.1	0.5	2.0	0.6	0.7
Statistical (stat)	0.6	0.5	3.4	1.7	2.5	1.6	0.8	0.7	0.5	3.4	0.7	2.2	0.9	2.6	0.5	0.5

of the B^0 decays taken in input are obtained from averages that assume isospin symmetry in decays of the $\Upsilon(4S)$ meson [39]. This symmetry is observed to hold with a precision of 1%–2%, and no uncertainty is assigned. However, it is noted that considering the correction suggested in Ref. [51] increases the value of $|V_{cb}|$ by 0.2×10^{-3} in both the CLN and BGL parametrizations.

The efficiency of the requirement that limits $m(K^+K^-)$ to be around the $\phi(1020)$ mass is evaluated using simulation. Given that the simulated model of the intermediate amplitudes contributing to the $D^-_{(s)} \to K^+K^-\pi^-$ decays may be inaccurate, a systematic uncertainty is estimated by comparing the efficiency of the $m(K^+K^-)$ requirement derived from simulation with that based on data from an independent control sample of $D^-_{(s)} \to K^+K^-\pi^-$ decays. The efficiency ratios $\xi^{(*)}$ change by a relative -4% when substituting the simulation-based efficiency of the $m(K^+K^-)$ requirement with that determined from data. This variation modifies the values of $|V_{cb}|$, $\mathcal{R}$ and $\mathcal{R}^*$ found in the fit, while producing negligible shifts to the form-factor parameters. The differences with respect to the nominal values are assigned as systematic uncertainties.

The knowledge of the physics backgrounds contributing to the inclusive $D_s^-\mu^+$ sample is limited by the lack of experimental measurements of exclusive semileptonic B_s^0 decays. These background components are, however, well separated in the $m_{\rm corr}$ versus $p_\perp(D_s^-)$ plane and their contribution is reduced to a few percent by the requirement $p_\perp(D_s^-)\ [\mathrm{GeV}/c] < 1.5 + 1.1 \times (m_{\rm corr}\ [\mathrm{GeV}/c^2] - 4.5)$ (dashed line in Fig. 2). To quantify by how much the assumed background composition can affect the determination of the parameters of interest, the fit is repeated by varying the requirements on the $m_{\rm corr}$ versus $p_\perp(D^-_{(s)})$ plane for both signal and reference samples. In the first variation, the more restrictive requirement $p_\perp(D^-_{(s)})\ [\mathrm{GeV}/c] < 0.7 + 4.0 \times (m_{\rm corr}\ [\mathrm{GeV}/c^2] - 4.5)$ is added on top of the baseline selection to further halve the expected background fractions. This requirement is shown as a dot-dashed line in Fig. 2, for the B_s^0 case. In the second variation, the baseline requirement is removed to allow maximum background contamination, which doubles with respect to that of the nominal selection. For both variations, the resulting samples are fit accounting for changes in the templates and in the efficiencies. The residuals for each parameter are computed as the difference between the values obtained in the alternative and baseline fits. The root-mean-square deviation of the residuals is taken as systematic uncertainty.

The analysis method is validated using large ensembles of pseudoexperiments, generated by resampling with repetitions (bootstrapping [52]) the samples of simulated signal and background decays and the same-sign data that model the combinatorial background. The relative proportions of signal and background components of the nominal fit to data are reproduced. Signal decays are generated by using both the CLN and BGL parametrizations with the form factors determined in the fit to data. Each sample is fit with the same form-factor parametrization used in the generation, and residuals between the fit and the generation values of each parameter are computed. The residuals that are observed to be at least two standard deviations different from zero are assigned as systematic uncertainties.

The simulated samples are corrected for mismodeling of the reconstruction and selection efficiency, of the response of the particle identification algorithms, and of the kinematic properties of the generated $B^0_{(s)}$ meson. A systematic uncertainty is assigned by varying the corrections within their uncertainties.

The measurement of $\mathcal{R}^{(*)}$ is performed only in the CLN parametrization, because, as shown in Fig. 6, the signal templates are marginally affected by the choice of the form-factor parametrization. Nevertheless, a systematic uncertainty is assigned as the shift in the $\mathcal{R}^{(*)}$ central values when fitting the data with the BGL parametrization.

The experimental systematic uncertainties are combined together, accounting for their correlations, in the middle section of Table VII. The correlations are reported in Appendix B.

As a consistency test, the fit is repeated by expressing the signal yields of the $B_s^0 \to D_s^-\mu^+\nu_\mu$ and $B_s^0 \to D_s^{*-}\mu^+\nu_\mu$ decays in terms of two different $|V_{cb}|$ parameters. The fit returns values of the two parameters in agreement with each other within one standard deviation.

Finally, a data-based null test of the analysis method is performed using a control sample of $B^0 \to D^{(*)-}\mu^+\nu_\mu$ decays where the D^- decays to the Cabibbo-favored $K^+\pi^-\pi^-$ final state. These decays are normalized to the same $B^0 \to D^{(*)-}\mu^+\nu_\mu$ decays, with $D^- \to [K^+K^-]_\phi\pi^-$, used in the default analysis to measure ratios of branching fractions between control and reference decays consistent with unity. The control sample is selected with criteria very similar to those of the reference sample, but the different D^- final state introduces differences between the efficiencies of the control and reference decays that are 40% larger than those between signal and reference decays. The control sample features the same fit components as described in Sec. VI for the reference sample, with signal and background decays modeled with simulation and combinatorial background with same-sign data. External inputs are changed to reflect the replacement of the signal with the control decays. Fits are performed using both the CLN and the BGL parametrizations. In both cases, the ratios of branching fractions between control and reference decays are all measured to be compatible with unity with 5%–6% relative precision.

IX. FINAL RESULTS AND CONCLUSIONS

A study of the $B_s^0 \to D_s^-\mu^+\nu_\mu$ and $B_s^0 \to D_s^{*-}\mu^+\nu_\mu$ decays is performed using proton-proton collision data

collected with the LHCb detector at center-of-mass energies of 7 and 8 TeV, corresponding to an integrated luminosity of 3 fb^{-1}. A novel analysis method is used to identify the two exclusive decay modes from the inclusive sample of selected $D_s^-\mu^+$ candidates and measure the CKM matrix element $|V_{cb}|$ using $B^0 \to D^-\mu^+\nu_\mu$ and $B^0 \to D^{*-}\mu^+\nu_\mu$ decays as normalization. The analysis is performed with both the CLN [2] and BGL [3–5] parametrizations to determine

$$|V_{cb}|_{\mathrm{CLN}} = (41.4 \pm 0.6(\mathrm{stat}) \pm 0.9(\mathrm{syst}) \pm 1.2(\mathrm{ext})) \times 10^{-3},$$
$$|V_{cb}|_{\mathrm{BGL}} = (42.3 \pm 0.8(\mathrm{stat}) \pm 0.9(\mathrm{syst}) \pm 1.2(\mathrm{ext})) \times 10^{-3},$$

where the first uncertainties are statistical (including contributions from both data and simulation), the second systematic, and the third due to the limited knowledge of the external inputs. The two results are compatible, when accounting for their correlation. These are the first determinations of $|V_{cb}|$ from exclusive decays at a hadron collider and the first using B_s^0 decays. The results are in agreement with the exclusive measurements based on B^0 and B^+ decays and as well with the inclusive determination [1].

The ratios of the branching fractions of the exclusive $B_s^0 \to D_s^{(*)-}\mu^+\nu_\mu$ decays relative to those of the exclusive $B^0 \to D^{(*)-}\mu^+\nu_\mu$ decays are measured to be

$$\mathcal{R} \equiv \frac{\mathcal{B}(B_s^0 \to D_s^-\mu^+\nu_\mu)}{\mathcal{B}(B^0 \to D^-\mu^+\nu_\mu)} = 1.09 \pm 0.05(\mathrm{stat}) \pm 0.06(\mathrm{syst}) \pm 0.05(\mathrm{ext}),$$
$$\mathcal{R}^* \equiv \frac{\mathcal{B}(B_s^0 \to D_s^{*-}\mu^+\nu_\mu)}{\mathcal{B}(B^0 \to D^{*-}\mu^+\nu_\mu)} = 1.06 \pm 0.05(\mathrm{stat}) \pm 0.07(\mathrm{syst}) \pm 0.05(\mathrm{ext}).$$

Taking the measured values of $\mathcal{B}(B^0 \to D^-\mu^+\nu_\mu)$ and $\mathcal{B}(B^0 \to D^{*-}\mu^+\nu_\mu)$ as additional inputs [39], the following exclusive branching fractions are determined for the first time:

$$\mathcal{B}(B_s^0 \to D_s^-\mu^+\nu_\mu) = (2.49 \pm 0.12(\mathrm{stat}) \pm 0.14(\mathrm{syst}) \pm 0.16(\mathrm{ext})) \times 10^{-2},$$
$$\mathcal{B}(B_s^0 \to D_s^{*-}\mu^+\nu_\mu) = (5.38 \pm 0.25(\mathrm{stat}) \pm 0.46(\mathrm{syst}) \pm 0.30(\mathrm{ext})) \times 10^{-2},$$

where the third uncertainties also include the contribution due to the limited knowledge of the normalization branching fractions. Finally, the ratio of $B_s^0 \to D_s^-\mu^+\nu_\mu$ to $B_s^0 \to D_s^{*-}\mu^+\nu_\mu$ branching fractions is determined to be

$$\frac{\mathcal{B}(B_s^0 \to D_s^-\mu^+\nu_\mu)}{\mathcal{B}(B_s^0 \to D_s^{*-}\mu^+\nu_\mu)} = 0.464 \pm 0.013(\mathrm{stat}) \pm 0.043(\mathrm{syst}).$$

The novel method employed in this analysis can also be used to measure $|V_{cb}|$ with semileptonic B^0 decays at LHCb. In this case, the uncertainty from the external inputs can be substantially decreased, as the dominant contribution in the current measurement is due to the knowledge of the B_s^0- to B^0-meson production ratio f_s/f_d. The limiting factor for B^0 decays stems from the knowledge of the reference decays branching fractions, but these are expected to improve from new measurements at the Belle II experiment [53].

ACKNOWLEDGMENTS

We express our gratitude to our colleagues in the CERN accelerator departments for the excellent performance of the LHC. We thank the technical and administrative staff at the LHCb institutes. We acknowledge support from CERN and from the national agencies: CAPES, CNPq, FAPERJ and FINEP (Brazil); MOST and NSFC (China); CNRS/IN2P3 (France); BMBF, DFG and MPG (Germany); INFN (Italy); NWO (Netherlands); MNiSW and NCN (Poland); MEN/IFA (Romania); MSHE (Russia); MinECo (Spain); SNSF and SER (Switzerland); NASU (Ukraine); STFC (United Kingdom); DOE NP and NSF (USA). We acknowledge the computing resources that are provided by CERN, IN2P3 (France), KIT and DESY (Germany), INFN (Italy), SURF (Netherlands), PIC (Spain), GridPP (United Kingdom), RRCKI and Yandex LLC (Russia), CSCS (Switzerland), IFIN-HH (Romania), CBPF (Brazil), PL-GRID (Poland) and OSC (USA). We are indebted to the communities behind the multiple open-source software packages on which we depend. Individual groups or members have received support from AvH Foundation (Germany); EPLANET, Marie Skłodowska-Curie Actions and ERC (European Union); ANR, Labex P2IO and OCEVU, and Région Auvergne-Rhône-Alpes (France); Key Research Program of Frontier Sciences of CAS, CAS PIFI, and the Thousand Talents Program (China); RFBR, RSF and Yandex LLC (Russia); GVA, XuntaGal and GENCAT (Spain); the Royal Society and the Leverhulme Trust (United Kingdom).

APPENDIX A: LATTICE QCD CALCULATION FOR $B_s^0 \to D_s^-\mu^+\nu_\mu$ FORM FACTORS

References [22,23] report LQCD calculations of the form-factor function over the full q^2 spectrum for $B_s^0 \to D_s^-\mu^+\nu_\mu$ decays. The calculations differ in the methodology and in the treatment of the sea quarks, with Ref. [22] using ensembles that include $2+1$ flavors and Ref. [23] using $2+1+1$ flavors. The two calculations agree.

The results reported in Ref. [23] are expressed in the BCL parametrization [6], with the series expanded up to

TABLE VIII. Coefficients of the $f_+(w)$ form factor in the BCL parametrization from Ref. [23].

		Covariance		
Parameter	Value	a_0^{BCL}	a_1^{BCL}	a_2^{BCL}
a_0^{BCL}	0.66574	0.00015	0.00022	0.00003
a_1^{BCL}	−3.23599		0.20443	0.10080
a_2^{BCL}	−0.07478			4.04413

order z^2 (see Appendix A of Ref. [23]). The parameters describing the $f_+(w)$ form factor are reported in Table VIII. To be used in this analysis, they need to be translated into the CLN and BGL parametrizations. For this purpose, 10^3 ensembles, each consisting of 10^7 q^2 values distributed according to $f_+(w)$, are generated by sampling the BCL parameters within their covariance. Each sample is then fit with the CLN and BGL equations of Sec. II to derive the corresponding set of parameters. Each fit parameter features a Gaussian distribution. The central value and uncertainty of each parameter are defined as the mean and the width of these distributions, respectively. In the CLN parametrization, the derived parameters are $\mathcal{G}(0) = 1.07 \pm 0.04$ and $\rho^2(D_s^-) = 1.23 \pm 0.05$, with a correlation of 84.2%. Both values are in agreement with the results reported in Ref. [22], $\mathcal{G}(0) = 1.068 \pm 0.040$ and $\rho^2(D_s^-) = 1.244 \pm 0.076$. (A combination is not attempted because of the unknown correlation between the two LQCD calculations.) In the BGL parametrization, the derived parameters are $\mathcal{G}(0) = 1.07 \pm 0.04$, $d_1 = -0.012 \pm 0.008$ and $d_2 = -0.24 \pm 0.05$, with correlation coefficients $\varrho(\mathcal{G}(0), d_1) = -82.4\%$, $\varrho(\mathcal{G}(0), d_2) = -37.2\%$ and $\varrho(d_1, d_2) = 10.0\%$.

APPENDIX B: DETAILED FIT RESULTS

Detailed results for the $|V_{cb}|$ fits, in both the CLN and BGL parametrizations, are reported in Table IX. The full correlation matrices are given in Tables X and XI, separately for the CLN and BGL configurations. Detailed results for the $\mathcal{R}$ and $\mathcal{R}^*$ fit are given in Table XII, with correlations in Table XIII.

TABLE IX. Detailed results for the $|V_{cb}|$ fits. The uncertainties on the free parameters include the statistical contribution and that due to the external inputs.

	Value		
Parameter	CLN fit	BGL fit	Constraint
$\lvert V_{cb}\rvert$ $[10^{-3}]$	41.4 ± 1.3	42.3 ± 1.4	Free
$\mathcal{G}(0)$	1.102 ± 0.034	1.094 ± 0.034	1.07 ± 0.04
$\rho^2(D_s^-)$	1.27 ± 0.05	⋯	1.23 ± 0.05
d_1	⋯	-0.017 ± 0.008	-0.012 ± 0.008
d_2	⋯	-0.26 ± 0.05	-0.24 ± 0.05
$h_{A_1}(1)$	0.899 ± 0.013	0.900 ± 0.013	0.902 ± 0.013
$\rho^2(D_s^{*-})$	1.23 ± 0.17	⋯	Free
$R_1(1)$	1.34 ± 0.25	⋯	Free
$R_2(1)$	0.83 ± 0.16	⋯	Free
a_0	⋯	0.037 ± 0.009	Free
a_1	⋯	0.28 ± 0.27	Free
b_1	⋯	-0.06 ± 0.07	Free
c_1	⋯	0.0031 ± 0.0023	Free
$f_s/f_d \times \mathcal{B}(D_s^- \to K^-K^+\pi^-) \times \tau$ [ps]	0.0191 ± 0.0008	0.0191 ± 0.0008	0.0191 ± 0.0008
$\mathcal{B}(D^- \to K^+K^-\pi^-)$	0.00993 ± 0.00024	0.00993 ± 0.00024	0.00993 ± 0.00024
$\mathcal{B}(D^{*-} \to D^-X)$	0.323 ± 0.006	0.323 ± 0.006	0.323 ± 0.006
$\mathcal{B}(B^0 \to D^-\mu^+\nu_\mu)$	0.0228 ± 0.0010	0.0230 ± 0.0010	0.0231 ± 0.0010
$\mathcal{B}(B^0 \to D^{*-}\mu^+\nu_\mu)$	0.0507 ± 0.0014	0.0506 ± 0.0014	0.0505 ± 0.0014
B_s^0 mass $[\mathrm{GeV}/c^2]$	5.36688 ± 0.00017	5.36688 ± 0.00017	5.36688 ± 0.00017
D_s^- mass $[\mathrm{GeV}/c^2]$	1.96834 ± 0.00007	1.96834 ± 0.00007	1.96834 ± 0.00007
D_s^{*-} mass $[\mathrm{GeV}/c^2]$	2.1122 ± 0.0004	2.1122 ± 0.0004	2.1122 ± 0.0004

TABLE X. Correlations (in percent) for the $|V_{cb}|$ fit in the CLN parametrization. The top section includes contributions from statistical sources and external inputs, the bottom section contributions from the experimental systematic uncertainties.

	$\mathcal{B}(D^- \to K^+K^-\pi^-)$	$\mathcal{B}(D^{*-} \to D^-X)$	$\mathcal{B}(B^0 \to D^-\mu^+\nu_\mu)$	$\mathcal{B}(B^0 \to D^{*-}\mu^+\nu_\mu)$	$R_1(1)$	$R_2(1)$	$\rho^2(D_s^-)$	$\mathcal{G}(0)$	$\rho^2(D_s^{*-})$	$h_{A_1}(1)$	η_{EW}	$\lvert V_{cb}\rvert$
$f_s/f_d \times \mathcal{B}(D_s^- \to K^-K^+\pi^-) \times \tau$	0.2	0.1	0.2	0.1	−0.1	0.1	0.0	−0.1	0.0	−0.1	−0.1	−62.1
$\mathcal{B}(D^- \to K^+K^-\pi^-)$		0.0	−0.1	−0.1	−0.1	0.0	0.0	0.0	0.0	0.1	0.1	38.0
$\mathcal{B}(D^{*-} \to D^-X)$			7.9	−4.7	2.4	−1.8	0.8	−2.8	1.9	5.0	0.0	17.4
$\mathcal{B}(B^0 \to D^-\mu^+\nu_\mu)$				11.2	−5.7	4.2	−1.9	6.8	−4.5	−11.8	0.0	33.9
$\mathcal{B}(B^0 \to D^{*-}\mu^+\nu_\mu)$					3.4	−2.5	1.1	−4.0	2.7	7.1	0.0	24.6
$R_1(1)$						−87.5	−2.5	0.4	89.1	−3.6	0.0	−10.3
$R_2(1)$							−18.0	−16.8	−96.6	2.7	0.0	10.1
$\rho^2(D_s^-)$								83.8	15.9	−1.1	0.0	−3.1
$\mathcal{G}(0)$									15.1	4.2	0.0	−17.3
$\rho^2(D_s^{*-})$										−2.8	0.0	−5.9
$h_{A_1}(1)$											0.0	−26.0
η_{EW}												−15.6
$R_1(1)$						−82.0	82.0	91.9	92.0	0.0	0.0	−26.8
$R_2(1)$							−100.0	−97.9	−53.1	0.0	0.0	3.3
$\rho^2(D_s^-)$								97.9	53.0	0.0	0.0	−3.2
$\mathcal{G}(0)$									69.2	0.0	0.0	−11.7
$\rho^2(D_s^{*-})$										0.0	0.0	−37.5

TABLE XI. Correlations (in percent) for the $|V_{cb}|$ fit in the BGL parametrization. The top section includes contributions from statistical sources and external inputs, the bottom section contributions from the experimental systematic uncertainties.

	$\mathcal{B}(D^- \to K^+K^-\pi^-)$	$\mathcal{B}(D^{*-} \to D^-X)$	$\mathcal{B}(B^0 \to D^-\mu^+\nu_\mu)$	$\mathcal{B}(B^0 \to D^{*-}\mu^+\nu_\mu)$	a_0	c_1	d_1	d_2	$\mathcal{G}(0)$	b_1	a_1	$h_{A_1}(1)$	η_{EW}	$\lvert V_{cb}\rvert$
$f_s/f_d \times \mathcal{B}(D_s^- \to K^-K^+\pi^-) \times \tau$	0.2	0.1	0.2	0.1	−0.1	−0.2	0.0	0.0	−0.1	−0.2	0.2	−0.1	−0.1	−57.6
$\mathcal{B}(D^- \to K^+K^-\pi^-)$		0.0	−0.1	−0.1	0.1	0.1	0.0	0.0	0.0	0.1	−0.1	0.1	0.1	35.3
$\mathcal{B}(D^{*-} \to D^-X)$			6.1	−3.8	2.7	6.8	−2.2	−0.7	−0.3	5.2	−8.3	4.0	0.0	12.8
$\mathcal{B}(B^0 \to D^-\mu^+\nu_\mu)$				8.7	−6.1	−15.6	5.1	1.7	0.9	−12.1	19.1	−9.1	0.1	38.3
$\mathcal{B}(B^0 \to D^{*-}\mu^+\nu_\mu)$					3.8	9.6	−3.1	−1.0	−0.5	7.4	−11.7	5.6	0.0	18.0
a_0						43.3	−1.4	−3.4	4.4	−56.6	−3.5	−4.0	0.0	−10.4
c_1							−16.9	−11.0	22.3	28.9	−70.7	−10.1	−0.1	−37.5
d_1								1.8	−80.8	4.7	5.0	3.2	0.0	−0.5
d_2									−32.5	1.6	6.2	1.0	0.0	3.0
$\mathcal{G}(0)$										−0.2	−12.8	0.5	0.0	−14.5
b_1											−77.9	−7.8	0.0	−26.1
a_1												12.3	0.1	37.2
$h_{A_1}(1)$													0.0	−18.9
η_{EW}														−14.5
a_0						−76.5	14.5	10.7	−5.8	−92.4	93.4	0.0	0.0	−6.4
c_1							−68.5	−65.6	61.7	78.8	−75.0	0.0	0.0	13.5
d_1								99.9	−99.6	−17.0	9.1	0.0	0.0	−15.1
d_2									−99.9	−13.2	5.2	0.0	0.0	−14.9
$\mathcal{G}(0)$										8.2	−0.1	0.0	0.0	14.6
b_1											−94.5	0.0	0.0	6.8
a_1												0.0	0.0	−5.7

TABLE XII. Detailed results for the $\mathcal{R}$ and $\mathcal{R}^*$ fit. The uncertainties on the free parameters include the statistical contribution and that due to the external inputs.

Parameter	Value	Constraint
$\mathcal{R}$	1.093 ± 0.074	Free
$\mathcal{R}^*$	1.059 ± 0.071	Free
$f_s/f_d \times \mathcal{B}(D_s^- \to K^-K^+\pi^-)$	0.0127 ± 0.0005	0.0127 ± 0.0005
$\mathcal{B}(D^- \to K^+K^-\pi^-)$	0.00993 ± 0.00024	0.00993 ± 0.00024
$\mathcal{B}(D^{*-} \to D^-X)$	0.323 ± 0.006	0.323 ± 0.006

TABLE XIII. Correlations (in percent) for the $\mathcal{R}$ and $\mathcal{R}^*$ fit. The top section includes contributions from statistical sources and external inputs, the bottom section contributions from the experimental systematic uncertainties.

	$\mathcal{B}(D^- \to K^+K^-\pi^-)$	$\mathcal{B}(D^{*-} \to D^-X)$	$\mathcal{R}$	$\mathcal{R}^*$
$f_s/f_d \times \mathcal{B}(D_s^- \to K^-K^+\pi^-)$	0.1	0.1	−58.1	−58.8
$\mathcal{B}(D^- \to K^+K^-\pi^-)$		0.0	35.5	36.0
$\mathcal{B}(D^{*-} \to D^-X)$			0.0	29.4
$\mathcal{R}$				14.0
$\mathcal{R}$				18.9

[1] Y. Amhis *et al.* (Heavy Flavor Averaging Group), Averages of b-hadron, c-hadron, and τ-lepton properties as of summer 2018, arXiv:1909.12524, updated results and plots available at https://hflav.web.cern.ch.

[2] I. Caprini, L. Lellouch, and M. Neubert, Dispersive bounds on the shape of $\bar{B} \to D^{(*)}\ell\bar{\nu}$ form factors, Nucl. Phys. **B530**, 153 (1998).

[3] C. G. Boyd, B. Grinstein, and R. F. Lebed, Constraints on Form Factors for Exclusive Semileptonic Heavy to Light Meson Decays, Phys. Rev. Lett. **74**, 4603 (1995).

[4] C. G. Boyd, B. Grinstein, and R. F. Lebed, Model-independent determinations of $\bar{B} \to D\ell\bar{\nu}$, $D^*\ell\bar{\nu}$ form factors, Nucl. Phys. **B461**, 493 (1996).

[5] C. G. Boyd, B. Grinstein, and R. F. Lebed, Precision corrections to dispersive bounds on form factors, Phys. Rev. D **56**, 6895 (1997).

[6] C. Bourrely, I. Caprini, and L. Lellouch, Model-independent description of $B \to \pi\ell\nu$ decays and a determination of $|V_{ub}|$, Phys. Rev. D **79**, 013008 (2009); Erratum, Phys. Rev. D **82**, 099902 (2010).

[7] F. U. Bernlochner, Z. Ligeti, M. Papucci, and D. J. Robinson, Tensions and correlations in $|V_{cb}|$ determinations, Phys. Rev. D **96**, 091503 (2017).

[8] D. Bigi, P. Gambino, and S. Schacht, A fresh look at the determination of $|V_{cb}|$ from $B \to D^*\ell\nu$, Phys. Lett. B **769**, 441 (2017).

[9] B. Grinstein and A. Kobach, Model-independent extraction of $|V_{cb}|$ from $\bar{B} \to D^*\ell\bar{\nu}$, Phys. Lett. B **771**, 359 (2017).

[10] S. Jaiswal, S. Nandi, and S. K. Patra, Extraction of $|V_{cb}|$ from $B \to D^{(*)}\ell\nu_\ell$ and the Standard Model predictions of $R(D^{(*)})$, J. High Energy Phys. 12 (2017) 060.

[11] P. Colangelo and F. De Fazio, Scrutinizing $\bar{B} \to D^*(D\pi)\ell^-\bar{\nu}_\ell$ and $\bar{B} \to D^*(D\gamma)\ell^-\bar{\nu}_\ell$ in search of new physics footprints, J. High Energy Phys. 06 (2018) 082.

[12] E. Waheed *et al.* (Belle Collaboration), Measurement of the CKM matrix element $|V_{cb}|$ from $B^0 \to D^{*-}\ell^+\nu_\ell$ at Belle, Phys. Rev. D **100**, 052007 (2019).

[13] J. P. Lees *et al.* (*BABAR* Collaboration), Extraction of Form Factors from a Four-Dimensional Angular Analysis of $\bar{B} \to D^*\ell^-\bar{\nu}_\ell$, Phys. Rev. Lett. **123**, 091801 (2019).

[14] P. Gambino, M. Jung, and S. Schacht, The V_{cb} puzzle: An update, Phys. Lett. B **795**, 386 (2019).

[15] M. Bordone, M. Jung, and D. van Dyk, Theory determination of $\bar{B} \to D^{(*)}\ell^-\bar{\nu}$ form factors at $\mathcal{O}(1/m_c^2)$, Eur. Phys. J. C **80**, 74 (2020).

[16] M. Bordone, N. Gubernari, M. Jung, and D. van Dyk, Heavy-quark expansion for $\bar{B}_s \to D_s^{(*)}$ form factors and unitarity bounds beyond the $SU(3)_F$ limit, arXiv:1912.09335.

[17] D. King, M. Kirk, A. Lenz, and T. Rauh, $|V_{cb}|$ and γ from B-mixing, arXiv:1911.07856.

[18] E. McLean, C. T. H. Davies, A. T. Lytle, and J. Koponen (HPQCD Collaboration), Lattice QCD form factor for $B_s^0 \to D_s^*\ell\nu$ at zero recoil with non-perturbative current renormalisation, Phys. Rev. D **99**, 114512 (2019).

[19] J. Harrison, C. Davies, and M. Wingate (HPQCD Collaboration), Lattice QCD calculation of the $B_{(s)} \to D_{(s)}^*\ell\nu$ form factors at zero recoil and implications for $|V_{cb}|$, Phys. Rev. D **97**, 054502 (2018).

[20] M. Atoui, V. Morénas, D. Bečirevic, and F. Sanfilippo, $B_s \to D_s\ell\nu_\ell$ near zero recoil in and beyond the Standard Model, Eur. Phys. J. C **74**, 2861 (2014).

[21] J. Flynn *et al.*, Form factors for semi-leptonic B decays, Proc. Sci. LATTICE2016 (**2016**) 296 [arXiv:1612.05112].

[22] C. J. Monahan, H. Na, C. M. Bouchard, G. P. Lepage, and J. Shigemitsu, $B_s \to D_s \ell \nu$ form factors and the fragmentation fraction ratio f_s/f_d, Phys. Rev. D **95**, 114506 (2017).

[23] E. McLean, C. T. H. Davies, J. Koponen, and A. T. Lytle, $B_s \to D_s \ell \nu$ form factors for the full q^2 range from Lattice QCD with non-perturbatively normalized currents, arXiv:1906.00701.

[24] R. Aaij *et al.* (LHCb Collaboration), Measurement of b-hadron fractions in 13 TeV pp collisions, Phys. Rev. D **100**, 031102 (2019).

[25] I. I. Bigi, T. Mannel, and N. Uraltsev, Semileptonic width ratios among beauty hadrons, J. High Energy Phys. 09 (2011) 012.

[26] A. Sirlin, Large m_W, m_Z behaviour of the $O(\alpha)$ corrections to semileptonic processes mediated by W, Nucl. Phys. **B196**, 83 (1982).

[27] D. Bigi and P. Gambino, Revisiting $B \to D \ell \nu$, Phys. Rev. D **94**, 094008 (2016).

[28] M. Neubert, Model-independent extraction of $|V_{cb}|$ from semi-leptonic decays, Phys. Lett. B **264**, 455 (1991).

[29] A. A. Alves, Jr. *et al.* (LHCb Collaboration), The LHCb detector at the LHC, J. Instrum. **3**, S08005 (2008).

[30] R. Aaij *et al.* (LHCb Collaboration), LHCb detector performance, Int. J. Mod. Phys. A **30**, 1530022 (2015).

[31] T. Sjöstrand, S. Mrenna, and P. Skands, PYTHIA 6.4 physics and manual, J. High Energy Phys. 05 (2006) 026; A brief introduction to PYTHIA 8.1, Comput. Phys. Commun. **178**, 852 (2008).

[32] I. Belyaev *et al.*, Handling of the generation of primary events in Gauss, the LHCb simulation framework, J. Phys. Conf. Ser. **331**, 032047 (2011).

[33] D. J. Lange, The EvtGen particle decay simulation package, Nucl. Instrum. Methods Phys. Res., Sect. A **462**, 152 (2001).

[34] P. Golonka and Z. Was, PHOTOS Monte Carlo: A precision tool for QED corrections in Z and W decays, Eur. Phys. J. C **45**, 97 (2006).

[35] J. Allison *et al.* (GEANT4 Collaboration), GEANT4 developments and applications, IEEE Trans. Nucl. Sci. **53**, 270 (2006); S. Agostinelli *et al.* (GEANT4 Collaboration), GEANT4: A simulation toolkit, Nucl. Instrum. Methods Phys. Res., Sect. A **506**, 250 (2003).

[36] M. Clemencic, G. Corti, S. Easo, C. R. Jones, S. Miglioranzi, M. Pappagallo, and P. Robbe, The LHCb simulation application, Gauss: Design, evolution and experience, J. Phys. Conf. Ser. **331**, 032023 (2011).

[37] R. Aaij *et al.* (LHCb Collaboration), Measurement of B_s^0 and D_s^- Meson Lifetimes, Phys. Rev. Lett. **119**, 101801 (2017).

[38] R. Aaij *et al.*, The LHCb trigger and its performance in 2011, J. Instrum. **8**, P04022 (2013).

[39] M. Tanabashi *et al.* (Particle Data Group), Review of particle physics, Phys. Rev. D **98**, 030001 (2018).

[40] K. Kodama *et al.* (Fermilab E653 Collaboration), Limits for four- and five-prong semimuonic charm meson decays, Phys. Lett. B **313**, 260 (1993).

[41] E. M. Aitala *et al.* (E791 Collaboration), Measurement of the form-factor ratios for $D^+ \to \bar{K}^{*0} \ell^+ \nu_\ell$, Phys. Lett. B **440**, 435 (1998).

[42] J. M. Link *et al.* (FOCUS Collaboration), Analysis of the semileptonic decay $D^0 \to \bar{K}^0 \pi^- \mu^+ \nu_\mu$, Phys. Lett. B **607**, 67 (2005).

[43] S. Dambach, U. Langenegger, and A. Starodumov, Neutrino reconstruction with topological information, Nucl. Instrum. Methods Phys. Res., Sect. A **569**, 824 (2006).

[44] G. Ciezarek, A. Lupato, M. Rotondo, and M. Vesterinen, Reconstruction of semileptonically decaying beauty hadrons produced in high energy pp collisions, J. High Energy Phys. 02 (2017) 021.

[45] S. Stone and L. Zhang, Method of studying Λ_b^0 decays with one missing particle, Adv. High Energy Phys. **2014**, 931257 (2014).

[46] R. Aaij *et al.* (LHCb Collaboration), Determination of the quark coupling strength $|V_{ub}|$ using baryonic decays, Nat. Phys. **11**, 743 (2015).

[47] R. Aaij *et al.* (LHCb Collaboration), Measurement of the shape of the $\Lambda_b^0 \to \Lambda_c^+ \mu^- \bar{\nu}_\mu$ differential decay rate, Phys. Rev. D **96**, 112005 (2017).

[48] R. Aaij *et al.* (LHCb Collaboration), Test of lepton flavor universality by the measurement of the $B^0 \to D^{*-} \tau^+ \nu_\tau$ branching fraction using three-prong τ decays, Phys. Rev. D **97**, 072013 (2018).

[49] R. Aaij *et al.* (LHCb Collaboration), Measurement of the relative $B^- \to D^0/D^{*0}/D^{**0} \mu^- \bar{\nu}_\mu$ branching fractions using B^- mesons from $\bar{B}_{s2}^{*0}$ decays, Phys. Rev. D **99**, 092009 (2019).

[50] R. Aaij *et al.* (LHCb Collaboration), Measurement of f_s/f_u variation with proton-proton collision energy and kinematics, Phys. Rev. Lett. **124**, 122002 (2020).

[51] M. Jung, Branching ratio measurements and isospin violation in B-meso decays, Phys. Lett. B **753**, 187 (2016).

[52] B. Efron, Bootstrap methods: Another look at the jackknife, Ann. Stat. **7**, 1 (1979).

[53] W. Altmannshofer *et al.* (Belle II Collaboration), The Belle II physics book, Prog. Theor. Exp. Phys. **2019**, 123C01 (2019).

R. Aaij,[31] C. Abellán Beteta,[49] T. Ackernley,[59] B. Adeva,[45] M. Adinolfi,[53] H. Afsharnia,[9] C. A. Aidala,[80] S. Aiola,[25] Z. Ajaltouni,[9] S. Akar,[66] P. Albicocco,[22] J. Albrecht,[14] F. Alessio,[47] M. Alexander,[58] A. Alfonso Albero,[44] G. Alkhazov,[37] P. Alvarez Cartelle,[60] A. A. Alves Jr.,[45] S. Amato,[2] Y. Amhis,[11] L. An,[21] L. Anderlini,[21] G. Andreassi,[48] M. Andreotti,[20] F. Archilli,[16] J. Arnau Romeu,[10] A. Artamonov,[43] M. Artuso,[67] K. Arzymatov,[41] E. Aslanides,[10] M. Atzeni,[49] B. Audurier,[26] S. Bachmann,[16] J. J. Back,[55] S. Baker,[60] V. Balagura,[11,a] W. Baldini,[20,47] A. Baranov,[41] R. J. Barlow,[61] S. Barsuk,[11] W. Barter,[60] M. Bartolini,[23,47,b] F. Baryshnikov,[77] G. Bassi,[28] V. Batozskaya,[35] B. Batsukh,[67] A. Battig,[14] A. Bay,[48] M. Becker,[14] F. Bedeschi,[28] I. Bediaga,[1] A. Beiter,[67] L. J. Bel,[31] V. Belavin,[41] S. Belin,[26] N. Beliy,[5] V. Bellee,[48] K. Belous,[43]

I. Belyaev,[38] G. Bencivenni,[22] E. Ben-Haim,[12] S. Benson,[31] S. Beranek,[13] A. Berezhnoy,[39] R. Bernet,[49] D. Berninghoff,[16] H. C. Bernstein,[67] C. Bertella,[47] E. Bertholet,[12] A. Bertolin,[27] C. Betancourt,[49] F. Betti,[19,c] M. O. Bettler,[54] Ia. Bezshyiko,[49] S. Bhasin,[53] J. Bhom,[33] M. S. Bieker,[14] S. Bifani,[52] P. Billoir,[12] A. Bizzeti,[21,d] M. Bjørn,[62] M. P. Blago,[47] T. Blake,[55] F. Blanc,[48] S. Blusk,[67] D. Bobulska,[58] V. Bocci,[30] O. Boente Garcia,[45] T. Boettcher,[63] A. Boldyrev,[78] A. Bondar,[42,e] N. Bondar,[37] S. Borghi,[61,47] M. Borisyak,[41] M. Borsato,[16] J. T. Borsuk,[33] T. J. V. Bowcock,[59] C. Bozzi,[20] M. J. Bradley,[60] S. Braun,[16] A. Brea Rodriguez,[45] M. Brodski,[47] J. Brodzicka,[33] A. Brossa Gonzalo,[55] D. Brundu,[26] E. Buchanan,[53] A. Buonaura,[49] C. Burr,[47] A. Bursche,[26] J. S. Butter,[31] J. Buytaert,[47] W. Byczynski,[47] S. Cadeddu,[26] H. Cai,[72] R. Calabrese,[20,f] L. Calero Diaz,[22] S. Cali,[22] R. Calladine,[52] M. Calvi,[24,g] M. Calvo Gomez,[44,h] P. Camargo Magalhaes,[53] A. Camboni,[44,h] P. Campana,[22] D. H. Campora Perez,[31] L. Capriotti,[19,c] A. Carbone,[19,c] G. Carboni,[29] R. Cardinale,[23,b] A. Cardini,[26] P. Carniti,[24,g] K. Carvalho Akiba,[31] A. Casais Vidal,[45] G. Casse,[59] M. Cattaneo,[47] G. Cavallero,[47] S. Celani,[48] R. Cenci,[28,i] J. Cerasoli,[10] M. G. Chapman,[53] M. Charles,[12,47] Ph. Charpentier,[47] G. Chatzikonstantinidis,[52] M. Chefdeville,[8] V. Chekalina,[41] C. Chen,[3] S. Chen,[26] A. Chernov,[33] S.-G. Chitic,[47] V. Chobanova,[45] M. Chrzaszcz,[33] A. Chubykin,[37] P. Ciambrone,[22] M. F. Cicala,[55] X. Cid Vidal,[45] G. Ciezarek,[47] F. Cindolo,[19] P. E. L. Clarke,[57] M. Clemencic,[47] H. V. Cliff,[54] J. Closier,[47] J. L. Cobbledick,[61] V. Coco,[47] J. A. B. Coelho,[11] J. Cogan,[10] E. Cogneras,[9] L. Cojocariu,[36] P. Collins,[47] T. Colombo,[47] A. Comerma-Montells,[16] A. Contu,[26] N. Cooke,[52] G. Coombs,[58] S. Coquereau,[44] G. Corti,[47] C. M. Costa Sobral,[55] B. Couturier,[47] D. C. Craik,[63] J. Crkovska,[66] A. Crocombe,[55] M. Cruz Torres,[1,j] R. Currie,[57] C. L. Da Silva,[66] E. Dall'Occo,[14] J. Dalseno,[45,53] C. D'Ambrosio,[47] A. Danilina,[38] P. d'Argent,[16] A. Davis,[61] O. De Aguiar Francisco,[47] K. De Bruyn,[47] S. De Capua,[61] M. De Cian,[48] J. M. De Miranda,[1] L. De Paula,[2] M. De Serio,[18,k] P. De Simone,[22] J. A. de Vries,[31] C. T. Dean,[66] W. Dean,[80] D. Decamp,[8] L. Del Buono,[12] B. Delaney,[54] H.-P. Dembinski,[15] M. Demmer,[14] A. Dendek,[34] V. Denysenko,[49] D. Derkach,[78] O. Deschamps,[9] F. Desse,[11] F. Dettori,[26,l] B. Dey,[7] A. Di Canto,[47] P. Di Nezza,[22] S. Didenko,[77] H. Dijkstra,[47] V. Dobishuk,[51] F. Dordei,[26] M. Dorigo,[28,m] A. C. dos Reis,[1] L. Douglas,[58] A. Dovbnya,[50] K. Dreimanis,[59] M. W. Dudek,[33] L. Dufour,[47] G. Dujany,[12] P. Durante,[47] J. M. Durham,[66] D. Dutta,[61] M. Dziewiecki,[16] A. Dziurda,[33] A. Dzyuba,[37] S. Easo,[56] U. Egede,[69] V. Egorychev,[38] S. Eidelman,[42,e] S. Eisenhardt,[57] R. Ekelhof,[14] S. Ek-In,[48] L. Eklund,[58] S. Ely,[67] A. Ene,[36] E. Epple,[66] S. Escher,[13] S. Esen,[31] T. Evans,[47] A. Falabella,[19] J. Fan,[3] N. Farley,[52] S. Farry,[59] D. Fazzini,[11] P. Fedin,[38] M. Féo,[47] P. Fernandez Declara,[47] A. Fernandez Prieto,[45] F. Ferrari,[19,c] L. Ferreira Lopes,[48] F. Ferreira Rodrigues,[2] S. Ferreres Sole,[31] M. Ferrillo,[49] M. Ferro-Luzzi,[47] S. Filippov,[40] R. A. Fini,[18] M. Fiorini,[20,f] M. Firlej,[34] K. M. Fischer,[62] C. Fitzpatrick,[47] T. Fiutowski,[34] F. Fleuret,[11,a] M. Fontana,[47] F. Fontanelli,[23,b] R. Forty,[47] V. Franco Lima,[59] M. Franco Sevilla,[65] M. Frank,[47] C. Frei,[47] D. A. Friday,[58] J. Fu,[25,n] M. Fuehring,[14] W. Funk,[47] E. Gabriel,[57] A. Gallas Torreira,[45] D. Galli,[19,c] S. Gallorini,[27] S. Gambetta,[57] Y. Gan,[3] M. Gandelman,[2] P. Gandini,[25] Y. Gao,[4] L. M. Garcia Martin,[46] J. García Pardiñas,[49] B. Garcia Plana,[45] F. A. Garcia Rosales,[11] J. Garra Tico,[54] L. Garrido,[44] D. Gascon,[44] C. Gaspar,[47] D. Gerick,[16] E. Gersabeck,[61] M. Gersabeck,[61] T. Gershon,[55] D. Gerstel,[10] Ph. Ghez,[8] V. Gibson,[54] A. Gioventù,[45] O. G. Girard,[48] P. Gironella Gironell,[44] L. Giubega,[36] C. Giugliano,[20] K. Gizdov,[57] V. V. Gligorov,[12] C. Göbel,[70] D. Golubkov,[38] A. Golutvin,[60,77] A. Gomes,[1,o] P. Gorbounov,[38,6] I. V. Gorelov,[39] C. Gotti,[24,g] E. Govorkova,[31] J. P. Grabowski,[16] R. Graciani Diaz,[44] T. Grammatico,[12] L. A. Granado Cardoso,[47] E. Graugés,[44] E. Graverini,[48] G. Graziani,[21] A. Grecu,[36] R. Greim,[31] P. Griffith,[20] L. Grillo,[61] L. Gruber,[47] B. R. Gruberg Cazon,[62] C. Gu,[3] E. Gushchin,[40] A. Guth,[13] Yu. Guz,[43,47] T. Gys,[47] P. A. Günther,[16] T. Hadavizadeh,[62] G. Haefeli,[48] C. Haen,[47] S. C. Haines,[54] P. M. Hamilton,[65] Q. Han,[7] X. Han,[16] T. H. Hancock,[62] S. Hansmann-Menzemer,[16] N. Harnew,[62] T. Harrison,[59] R. Hart,[31] C. Hasse,[47] M. Hatch,[47] J. He,[5] M. Hecker,[60] K. Heijhoff,[31] K. Heinicke,[14] A. Heister,[14] A. M. Hennequin,[47] K. Hennessy,[59] L. Henry,[46] J. Heuel,[13] A. Hicheur,[68] D. Hill,[62] M. Hilton,[61] P. H. Hopchev,[48] J. Hu,[16] W. Hu,[7] W. Huang,[5] W. Hulsbergen,[31] T. Humair,[60] R. J. Hunter,[55] M. Hushchyn,[78] D. Hutchcroft,[59] D. Hynds,[31] P. Ibis,[14] M. Idzik,[34] P. Ilten,[52] A. Inglessi,[37] A. Inyakin,[43] K. Ivshin,[37] R. Jacobsson,[47] S. Jakobsen,[47] E. Jans,[31] B. K. Jashal,[46] A. Jawahery,[65] V. Jevtic,[14] F. Jiang,[3] M. John,[62] D. Johnson,[47] C. R. Jones,[54] B. Jost,[47] N. Jurik,[62] S. Kandybei,[50] M. Karacson,[47] J. M. Kariuki,[53] N. Kazeev,[78] M. Kecke,[16] F. Keizer,[54,47] M. Kelsey,[67] M. Kenzie,[55] T. Ketel,[32] B. Khanji,[47] A. Kharisova,[79] K. E. Kim,[67] T. Kirn,[13] V. S. Kirsebom,[48] S. Klaver,[22] K. Klimaszewski,[35] S. Koliiev,[51] A. Kondybayeva,[77] A. Konoplyannikov,[38] P. Kopciewicz,[34] R. Kopecna,[16] P. Koppenburg,[31] I. Kostiuk,[31,51] O. Kot,[51] S. Kotriakhova,[37] L. Kravchuk,[40] R. D. Krawczyk,[47] M. Kreps,[55] F. Kress,[60] S. Kretzschmar,[13] P. Krokovny,[42,e] W. Krupa,[34] W. Krzemien,[35] W. Kucewicz,[33,p] M. Kucharczyk,[33] V. Kudryavtsev,[42,e] H. S. Kuindersma,[31] G. J. Kunde,[66] T. Kvaratskheliya,[38] D. Lacarrere,[47] G. Lafferty,[61] A. Lai,[26] D. Lancierini,[49] J. J. Lane,[61] G. Lanfranchi,[22] C. Langenbruch,[13] O. Lantwin,[49] T. Latham,[55] F. Lazzari,[28,q] C. Lazzeroni,[52] R. Le Gac,[10] R. Lefèvre,[9]

A. Leflat,[39] O. Leroy,[10] T. Lesiak,[33] B. Leverington,[16] H. Li,[71] X. Li,[66] Y. Li,[6] Z. Li,[67] X. Liang,[67] R. Lindner,[47] V. Lisovskyi,[14] G. Liu,[71] X. Liu,[3] D. Loh,[55] A. Loi,[26] J. Lomba Castro,[45] I. Longstaff,[58] J. H. Lopes,[2] G. Loustau,[49] G. H. Lovell,[54] Y. Lu,[6] D. Lucchesi,[27,r] M. Lucio Martinez,[31] Y. Luo,[3] A. Lupato,[27] E. Luppi,[20,f] O. Lupton,[55] A. Lusiani,[28,s] X. Lyu,[5] S. Maccolini,[19,c] F. Machefert,[11] F. Maciuc,[36] V. Macko,[48] P. Mackowiak,[14] S. Maddrell-Mander,[53] L. R. Madhan Mohan,[53] O. Maev,[37,47] A. Maevskiy,[78] D. Maisuzenko,[37] M. W. Majewski,[34] S. Malde,[62] B. Malecki,[47] A. Malinin,[76] T. Maltsev,[42,e] H. Malygina,[16] G. Manca,[26,l] G. Mancinelli,[10] R. Manera Escalero,[44] D. Manuzzi,[19,c] D. Marangotto,[25,n] J. Maratas,[9,t] J. F. Marchand,[8] U. Marconi,[19] S. Mariani,[21] C. Marin Benito,[11] M. Marinangeli,[48] P. Marino,[48] J. Marks,[16] P. J. Marshall,[59] G. Martellotti,[30] L. Martinazzoli,[47] M. Martinelli,[24,g] D. Martinez Santos,[45] F. Martinez Vidal,[46] A. Massafferri,[1] M. Materok,[13] R. Matev,[47] A. Mathad,[49] Z. Mathe,[47] V. Matiunin,[38] C. Matteuzzi,[24] K. R. Mattioli,[80] A. Mauri,[49] E. Maurice,[11,a] M. McCann,[60] L. Mcconnell,[17] A. McNab,[61] R. McNulty,[17] J. V. Mead,[59] B. Meadows,[64] C. Meaux,[10] G. Meier,[14] N. Meinert,[74] D. Melnychuk,[35] S. Meloni,[24,g] M. Merk,[31] A. Merli,[25] M. Mikhasenko,[47] D. A. Milanes,[73] E. Millard,[55] M.-N. Minard,[8] O. Mineev,[38] L. Minzoni,[20,f] S. E. Mitchell,[57] B. Mitreska,[61] D. S. Mitzel,[47] A. Mödden,[14] A. Mogini,[12] R. D. Moise,[60] T. Mombächer,[14] I. A. Monroy,[73] S. Monteil,[9] M. Morandin,[27] G. Morello,[22] M. J. Morello,[28,s] J. Moron,[34] A. B. Morris,[10] A. G. Morris,[55] R. Mountain,[67] H. Mu,[3] F. Muheim,[57] M. Mukherjee,[7] M. Mulder,[31] D. Müller,[47] K. Müller,[49] V. Müller,[14] C. H. Murphy,[62] D. Murray,[61] P. Muzzetto,[26] P. Naik,[53] T. Nakada,[48] R. Nandakumar,[56] A. Nandi,[62] T. Nanut,[48] I. Nasteva,[2] M. Needham,[57] N. Neri,[25,n] S. Neubert,[16] N. Neufeld,[47] R. Newcombe,[60] T. D. Nguyen,[48] C. Nguyen-Mau,[48,u] E. M. Niel,[11] S. Nieswand,[13] N. Nikitin,[39] N. S. Nolte,[47] C. Nunez,[80] A. Oblakowska-Mucha,[34] V. Obraztsov,[43] S. Ogilvy,[58] D. P. O'Hanlon,[19] R. Oldeman,[26,l] C. J. G. Onderwater,[75] J. D. Osborn,[80] A. Ossowska,[33] J. M. Otalora Goicochea,[2] T. Ovsiannikova,[38] P. Owen,[49] A. Oyanguren,[46] P. R. Pais,[48] T. Pajero,[28,s] A. Palano,[18] M. Palutan,[22] G. Panshin,[79] A. Papanestis,[56] M. Pappagallo,[57] L. L. Pappalardo,[20,f] C. Pappenheimer,[64] W. Parker,[65] C. Parkes,[61] G. Passaleva,[21,47] A. Pastore,[18] M. Patel,[60] C. Patrignani,[19,c] A. Pearce,[47] A. Pellegrino,[31] M. Pepe Altarelli,[47] S. Perazzini,[19] D. Pereima,[38] P. Perret,[9] L. Pescatore,[48] K. Petridis,[53] A. Petrolini,[23,b] A. Petrov,[76] S. Petrucci,[57] M. Petruzzo,[25,n] B. Pietrzyk,[8] G. Pietrzyk,[48] M. Pili,[62] D. Pinci,[30] J. Pinzino,[47] F. Pisani,[47] A. Piucci,[16] V. Placinta,[36] S. Playfer,[57] J. Plews,[52] M. Plo Casasus,[45] F. Polci,[12] M. Poli Lener,[22] M. Poliakova,[67] A. Poluektov,[10] N. Polukhina,[77,v] I. Polyakov,[67] E. Polycarpo,[2] G. J. Pomery,[53] S. Ponce,[47] A. Popov,[43] D. Popov,[52] S. Poslavskii,[43] K. Prasanth,[33] L. Promberger,[47] C. Prouve,[45] V. Pugatch,[51] A. Puig Navarro,[49] H. Pullen,[62] G. Punzi,[28,i] W. Qian,[5] J. Qin,[5] R. Quagliani,[12] B. Quintana,[9] N. V. Raab,[17] R. I. Rabadan Trejo,[10] B. Rachwal,[34] J. H. Rademacker,[53] M. Rama,[28] M. Ramos Pernas,[45] M. S. Rangel,[2] F. Ratnikov,[41,78] G. Raven,[32] M. Reboud,[8] F. Redi,[48] F. Reiss,[12] C. Remon Alepuz,[46] Z. Ren,[3] V. Renaudin,[62] S. Ricciardi,[56] S. Richards,[53] K. Rinnert,[59] P. Robbe,[11] A. Robert,[12] A. B. Rodrigues,[48] E. Rodrigues,[64] J. A. Rodriguez Lopez,[73] M. Roehrken,[47] S. Roiser,[47] A. Rollings,[62] V. Romanovskiy,[43] M. Romero Lamas,[45] A. Romero Vidal,[45] J. D. Roth,[80] M. Rotondo,[22] M. S. Rudolph,[67] T. Ruf,[47] J. Ruiz Vidal,[46] J. Ryzka,[34] J. J. Saborido Silva,[45] N. Sagidova,[37] B. Saitta,[26,l] C. Sanchez Gras,[31] C. Sanchez Mayordomo,[46] R. Santacesaria,[30] C. Santamarina Rios,[45] M. Santimaria,[22] E. Santovetti,[29,w] G. Sarpis,[61] A. Sarti,[30] C. Satriano,[30,x] A. Satta,[29] M. Saur,[5] D. Savrina,[38,39] L. G. Scantlebury Smead,[62] S. Schael,[13] M. Schellenberg,[14] M. Schiller,[58] H. Schindler,[47] M. Schmelling,[15] T. Schmelzer,[14] B. Schmidt,[47] O. Schneider,[48] A. Schopper,[47] H. F. Schreiner,[64] M. Schubiger,[31] S. Schulte,[48] M. H. Schune,[11] R. Schwemmer,[47] B. Sciascia,[22] A. Sciubba,[30,y] S. Sellam,[68] A. Semennikov,[38] A. Sergi,[52,47] N. Serra,[49] J. Serrano,[10] L. Sestini,[27] A. Seuthe,[14] P. Seyfert,[47] D. M. Shangase,[80] M. Shapkin,[43] L. Shchutska,[48] T. Shears,[59] L. Shekhtman,[42,e] V. Shevchenko,[76,77] E. Shmanin,[77] J. D. Shupperd,[67] B. G. Siddi,[20] R. Silva Coutinho,[49] L. Silva de Oliveira,[2] G. Simi,[27,r] S. Simone,[18,k] I. Skiba,[20] N. Skidmore,[16] T. Skwarnicki,[67] M. W. Slater,[52] J. G. Smeaton,[54] A. Smetkina,[38] E. Smith,[13] I. T. Smith,[57] M. Smith,[60] A. Snoch,[31] M. Soares,[19] L. Soares Lavra,[1] M. D. Sokoloff,[64] F. J. P. Soler,[58] B. Souza De Paula,[2] B. Spaan,[14] E. Spadaro Norella,[25,n] P. Spradlin,[58] F. Stagni,[47] M. Stahl,[64] S. Stahl,[47] P. Stefko,[48] O. Steinkamp,[49] S. Stemmle,[16] O. Stenyakin,[43] M. Stepanova,[37] H. Stevens,[14] S. Stone,[67] S. Stracka,[28] M. E. Stramaglia,[48] M. Straticiuc,[36] S. Strokov,[79] J. Sun,[3] L. Sun,[72] Y. Sun,[65] P. Svihra,[61] K. Swientek,[34] A. Szabelski,[35] T. Szumlak,[34] M. Szymanski,[5] S. Taneja,[61] Z. Tang,[3] T. Tekampe,[14] G. Tellarini,[20] F. Teubert,[47] E. Thomas,[47] K. A. Thomson,[59] M. J. Tilley,[60] V. Tisserand,[9] S. T'Jampens,[8] M. Tobin,[6] S. Tolk,[47] L. Tomassetti,[20,f] D. Tonelli,[28] D. Torres Machado,[1] D. Y. Tou,[12] E. Tournefier,[8] M. Traill,[58] M. T. Tran,[48] C. Trippl,[48] A. Trisovic,[54] A. Tsaregorodtsev,[10] G. Tuci,[28,47,i] A. Tully,[48] N. Tuning,[31] A. Ukleja,[35] A. Usachov,[11] A. Ustyuzhanin,[41,78] U. Uwer,[16] A. Vagner,[79] V. Vagnoni,[19] A. Valassi,[47] G. Valenti,[19] M. van Beuzekom,[31] H. Van Hecke,[66] E. van Herwijnen,[47] C. B. Van Hulse,[17] M. van Veghel,[75] R. Vazquez Gomez,[44,22] P. Vazquez Regueiro,[45] C. Vázquez Sierra,[31] S. Vecchi,[20] J. J. Velthuis,[53] M. Veltri,[21,z]

A. Venkateswaran,[67] M. Vernet,[9] M. Veronesi,[31] M. Vesterinen,[55] J. V. Viana Barbosa,[47] D. Vieira,[5] M. Vieites Diaz,[48] H. Viemann,[74] X. Vilasis-Cardona,[44,h] A. Vitkovskiy,[31] V. Volkov,[39] A. Vollhardt,[49] D. Vom Bruch,[12] A. Vorobyev,[37] V. Vorobyev,[42,e] N. Voropaev,[37] R. Waldi,[74] J. Walsh,[28] J. Wang,[3] J. Wang,[72] J. Wang,[6] M. Wang,[3] Y. Wang,[7] Z. Wang,[49] D. R. Ward,[54] H. M. Wark,[59] N. K. Watson,[52] D. Websdale,[60] A. Weiden,[49] C. Weisser,[63] B. D. C. Westhenry,[53] D. J. White,[61] M. Whitehead,[13] D. Wiedner,[14] G. Wilkinson,[62] M. Wilkinson,[67] I. Williams,[54] M. Williams,[63] M. R. J. Williams,[61] T. Williams,[52] F. F. Wilson,[56] W. Wislicki,[35] M. Witek,[33] L. Witola,[16] G. Wormser,[11] S. A. Wotton,[54] H. Wu,[67] K. Wyllie,[47] Z. Xiang,[5] D. Xiao,[7] Y. Xie,[7] H. Xing,[71] A. Xu,[4] L. Xu,[3] M. Xu,[7] Q. Xu,[5] Z. Xu,[8] Z. Xu,[4] Z. Yang,[3] Z. Yang,[65] Y. Yao,[67] L. E. Yeomans,[59] H. Yin,[7] J. Yu,[7,aa] X. Yuan,[67] O. Yushchenko,[43] K. A. Zarebski,[52] M. Zavertyaev,[15,v] M. Zdybal,[33] M. Zeng,[3] D. Zhang,[7] L. Zhang,[3] S. Zhang,[4] W. C. Zhang,[3,bb] Y. Zhang,[47] A. Zhelezov,[16] Y. Zheng,[5] X. Zhou,[5] Y. Zhou,[5] X. Zhu,[3] V. Zhukov,[13,39] J. B. Zonneveld,[57] and S. Zucchelli[19,c]

(LHCb Collaboration)

[1]*Centro Brasileiro de Pesquisas Físicas (CBPF), Rio de Janeiro, Brazil*
[2]*Universidade Federal do Rio de Janeiro (UFRJ), Rio de Janeiro, Brazil*
[3]*Center for High Energy Physics, Tsinghua University, Beijing, China*
[4]*School of Physics State Key Laboratory of Nuclear Physics and Technology, Peking University, Beijing, China*
[5]*University of Chinese Academy of Sciences, Beijing, China*
[6]*Institute Of High Energy Physics (IHEP), Beijing, China*
[7]*Institute of Particle Physics, Central China Normal University, Wuhan, Hubei, China*
[8]*Univ. Grenoble Alpes, Univ. Savoie Mont Blanc, CNRS, IN2P3-LAPP, Annecy, France*
[9]*Université Clermont Auvergne, CNRS/IN2P3, LPC, Clermont-Ferrand, France*
[10]*Aix Marseille Univ, CNRS/IN2P3, CPPM, Marseille, France*
[11]*Université Paris-Saclay, CNRS/IN2P3, IJCLab, Orsay, France*
[12]*LPNHE, Sorbonne Université, Paris Diderot Sorbonne Paris Cité, CNRS/IN2P3, Paris, France*
[13]*I. Physikalisches Institut, RWTH Aachen University, Aachen, Germany*
[14]*Fakultät Physik, Technische Universität Dortmund, Dortmund, Germany*
[15]*Max-Planck-Institut für Kernphysik (MPIK), Heidelberg, Germany*
[16]*Physikalisches Institut, Ruprecht-Karls-Universität Heidelberg, Heidelberg, Germany*
[17]*School of Physics, University College Dublin, Dublin, Ireland*
[18]*INFN Sezione di Bari, Bari, Italy*
[19]*INFN Sezione di Bologna, Bologna, Italy*
[20]*INFN Sezione di Ferrara, Ferrara, Italy*
[21]*INFN Sezione di Firenze, Firenze, Italy*
[22]*INFN Laboratori Nazionali di Frascati, Frascati, Italy*
[23]*INFN Sezione di Genova, Genova, Italy*
[24]*INFN Sezione di Milano-Bicocca, Milano, Italy*
[25]*INFN Sezione di Milano, Milano, Italy*
[26]*INFN Sezione di Cagliari, Monserrato, Italy*
[27]*INFN Sezione di Padova, Padova, Italy*
[28]*INFN Sezione di Pisa, Pisa, Italy*
[29]*INFN Sezione di Roma Tor Vergata, Roma, Italy*
[30]*INFN Sezione di Roma La Sapienza, Roma, Italy*
[31]*Nikhef National Institute for Subatomic Physics, Amsterdam, Netherlands*
[32]*Nikhef National Institute for Subatomic Physics and VU University Amsterdam, Amsterdam, Netherlands*
[33]*Henryk Niewodniczanski Institute of Nuclear Physics Polish Academy of Sciences, Kraków, Poland*
[34]*AGH - University of Science and Technology, Faculty of Physics and Applied Computer Science, Kraków, Poland*
[35]*National Center for Nuclear Research (NCBJ), Warsaw, Poland*
[36]*Horia Hulubei National Institute of Physics and Nuclear Engineering, Bucharest-Magurele, Romania*
[37]*Petersburg Nuclear Physics Institute NRC Kurchatov Institute (PNPI NRC KI), Gatchina, Russia*
[38]*Institute of Theoretical and Experimental Physics NRC Kurchatov Institute (ITEP NRC KI), Moscow, Russia, Moscow, Russia*
[39]*Institute of Nuclear Physics, Moscow State University (SINP MSU), Moscow, Russia*
[40]*Institute for Nuclear Research of the Russian Academy of Sciences (INR RAS), Moscow, Russia*
[41]*Yandex School of Data Analysis, Moscow, Russia*

[42]*Budker Institute of Nuclear Physics (SB RAS), Novosibirsk, Russia*
[43]*Institute for High Energy Physics NRC Kurchatov Institute (IHEP NRC KI), Protvino, Russia, Protvino, Russia*
[44]*ICCUB, Universitat de Barcelona, Barcelona, Spain*
[45]*Instituto Galego de Física de Altas Enerxías (IGFAE), Universidade de Santiago de Compostela, Santiago de Compostela, Spain*
[46]*Instituto de Fisica Corpuscular, Centro Mixto Universidad de Valencia - CSIC, Valencia, Spain*
[47]*European Organization for Nuclear Research (CERN), Geneva, Switzerland*
[48]*Institute of Physics, Ecole Polytechnique Fédérale de Lausanne (EPFL), Lausanne, Switzerland*
[49]*Physik-Institut, Universität Zürich, Zürich, Switzerland*
[50]*NSC Kharkiv Institute of Physics and Technology (NSC KIPT), Kharkiv, Ukraine*
[51]*Institute for Nuclear Research of the National Academy of Sciences (KINR), Kyiv, Ukraine*
[52]*University of Birmingham, Birmingham, United Kingdom*
[53]*H.H. Wills Physics Laboratory, University of Bristol, Bristol, United Kingdom*
[54]*Cavendish Laboratory, University of Cambridge, Cambridge, United Kingdom*
[55]*Department of Physics, University of Warwick, Coventry, United Kingdom*
[56]*STFC Rutherford Appleton Laboratory, Didcot, United Kingdom*
[57]*School of Physics and Astronomy, University of Edinburgh, Edinburgh, United Kingdom*
[58]*School of Physics and Astronomy, University of Glasgow, Glasgow, United Kingdom*
[59]*Oliver Lodge Laboratory, University of Liverpool, Liverpool, United Kingdom*
[60]*Imperial College London, London, United Kingdom*
[61]*Department of Physics and Astronomy, University of Manchester, Manchester, United Kingdom*
[62]*Department of Physics, University of Oxford, Oxford, United Kingdom*
[63]*Massachusetts Institute of Technology, Cambridge, Massachusetts, USA*
[64]*University of Cincinnati, Cincinnati, Ohio, USA*
[65]*University of Maryland, College Park, Maryland, USA*
[66]*Los Alamos National Laboratory (LANL), Los Alamos, New Mexico, USA*
[67]*Syracuse University, Syracuse, New York, USA*
[68]*Laboratory of Mathematical and Subatomic Physics, Constantine, Algeria [associated with Universidade Federal do Rio de Janeiro (UFRJ), Rio de Janeiro, Brazil]*
[69]*School of Physics and Astronomy, Monash University, Melbourne, Australia (associated with Department of Physics, University of Warwick, Coventry, United Kingdom)*
[70]*Pontifícia Universidade Católica do Rio de Janeiro (PUC-Rio), Rio de Janeiro, Brazil [associated with Universidade Federal do Rio de Janeiro (UFRJ), Rio de Janeiro, Brazil]*
[71]*South China Normal University, Guangzhou, China (associated with Center for High Energy Physics, Tsinghua University, Beijing, China)*
[72]*School of Physics and Technology, Wuhan University, Wuhan, China (associated with Center for High Energy Physics, Tsinghua University, Beijing, China)*
[73]*Departamento de Fisica, Universidad Nacional de Colombia, Bogota, Colombia (associated with LPNHE, Sorbonne Université, Paris Diderot Sorbonne Paris Cité, CNRS/IN2P3, Paris, France)*
[74]*Institut für Physik, Universität Rostock, Rostock, Germany (associated with Physikalisches Institut, Ruprecht-Karls-Universität Heidelberg, Heidelberg, Germany)*
[75]*Van Swinderen Institute, University of Groningen, Groningen, Netherlands (associated with Nikhef National Institute for Subatomic Physics, Amsterdam, Netherlands)*
[76]*National Research Centre Kurchatov Institute, Moscow, Russia [associated with Institute of Theoretical and Experimental Physics NRC Kurchatov Institute (ITEP NRC KI), Moscow, Russia, Moscow, Russia]*
[77]*National University of Science and Technology "MISIS", Moscow, Russia [associated with Institute of Theoretical and Experimental Physics NRC Kurchatov Institute (ITEP NRC KI), Moscow, Russia, Moscow, Russia]*
[78]*National Research University Higher School of Economics, Moscow, Russia (associated with Yandex School of Data Analysis, Moscow, Russia)*
[79]*National Research Tomsk Polytechnic University, Tomsk, Russia [associated with Institute of Theoretical and Experimental Physics NRC Kurchatov Institute (ITEP NRC KI), Moscow, Russia, Moscow, Russia]*
[80]*University of Michigan, Ann Arbor, USA (associated with Syracuse University, Syracuse, New York, USA)*

[a]Also at Laboratoire Leprince-Ringuet, Palaiseau, France.
[b]Also at Università di Genova, Genova, Italy.
[c]Also at Università di Bologna, Bologna, Italy.
[d]Also at Università di Modena e Reggio Emilia, Modena, Italy.
[e]Also at Novosibirsk State University, Novosibirsk, Russia.
[f]Also at Università di Ferrara, Ferrara, Italy.
[g]Also at Università di Milano Bicocca, Milano, Italy.
[h]Also at DS4DS, La Salle, Universitat Ramon Llull, Barcelona, Spain.
[i]Also at Università di Pisa, Pisa, Italy.
[j]Also at Universidad Nacional Autonoma de Honduras, Tegucigalpa, Honduras.
[k]Also at Università di Bari, Bari, Italy.
[l]Also at Università di Cagliari, Cagliari, Italy.
[m]Also at INFN Sezione di Trieste, Trieste, Italy.
[n]Also at Università degli Studi di Milano, Milano, Italy.
[o]Also at Universidade Federal do Triângulo Mineiro (UFTM), Uberaba-MG, Brazil.
[p]Also at AGH - University of Science and Technology, Faculty of Computer Science, Electronics and Telecommunications, Kraków, Poland.
[q]Also at Università di Siena, Siena, Italy.
[r]Also at Università di Padova, Padova, Italy.
[s]Also at Scuola Normale Superiore, Pisa, Italy.
[t]Also at MSU - Iligan Institute of Technology (MSU-IIT), Iligan, Philippines.
[u]Also at Hanoi University of Science, Hanoi, Vietnam.
[v]Also at P.N. Lebedev Physical Institute, Russian Academy of Science (LPI RAS), Moscow, Russia.
[w]Also at Università di Roma Tor Vergata, Roma, Italy.
[x]Also at Università della Basilicata, Potenza, Italy.
[y]Also at Università di Roma La Sapienza, Roma, Italy.
[z]Also at Università di Urbino, Urbino, Italy.
[aa]Also at Physics and Micro Electronic College, Hunan University, Changsha City, China.
[bb]Also at School of Physics and Information Technology, Shaanxi Normal University (SNNU), Xi'an, China.